Master Equation Study of Hydrogen Abstraction from HCHO by OH Via a Chemically Activated Intermediate

Rui Ming Zhang[a,&], Wenqi Chen[a,&], Donald G. Truhlar[b,*] and Xuefei Xu [a,*]

a *Center for Combustion Energy, Department of Energy and Power Engineering, and Key Laboratory for Thermal Science and Power Engineering of Ministry of Education, Tsinghua University, Beijing 100084, China*

b *Department of Chemistry, Chemical Theory Center, and Minnesota Supercomputing Institute, University of Minnesota, Minneapolis, Minnesota 55455-0431, USA*

& *These authors contributed equally to this work and are co-first authors.*

E-mails: xuxuefei@tsinghua.edu.cn; truhlar@umn.edu

ABSTRACT: The abstraction reaction of hydrogen from formaldehyde by OH radical plays an important role in formaldehyde oxidation. The reaction involves a bimolecular association to form a chemically activated hydrogen-bonded reaction complex followed by a unimolecular reaction of the complex to generate the products. The reaction rate is usually considered to be pressure-independent by assuming equilibrium between the reactants and the complex. However, our nonequilibrium calculations based on the chemically significant eigenmode of the master equation, carried out with our recently developed *TUMME* program, indicate that the reaction complex makes the rate constant dependent on pressure at low temperatures (T < 200 K). The calculations include anharmonicity, variational effects, and multi-dimensional tunneling. We find that the reaction rate constant reaches a low-pressure limit at pressures below 10 Torr over the whole investigated temperature range (20 K – 1800 K), which explains why the available low-temperature experiments, which are for pressures below 2 Torr, did not observe the pressure dependence. A new extension of the *TUMME* master-equation program is used to explore the time evolutions of the concentrations of the OH radical and the complex under pseudo-first-order conditions. The time-dependent evolution of the concentrations of the complex at a low temperature provides direct evidence for the stabilization of the reaction complex at high pressures, and it shows the negligible role of stabilized reaction complex at low pressures. The picture that emerges is qualitatively consistent with our previous study of the reaction of methanol with OH in that the tunneling in the unimolecular step from the complex to the products affects the phenomenological reaction rate constants differently at high and low pressures and leads to a significant pressure effect.

1. Introduction

Formaldehyde (HCHO) plays an important role in tropospheric chemistry, and it is an intermediate in combustion and forest fires. Formaldehyde reactions are of particular interest for understanding the combustion kinetics of oxygenated fuels.[1] In the atmosphere, formaldehyde pollutants can lead to the formation of ground-level ozone, photochemical oxidants, and photochemical smog,[2] and it is hazardous to human health. Additionally, formaldehyde is the first organic polyatomic molecule observed in the interstellar medium,[3] and reactions involving formaldehyde have received much attention in ultracold interstellar chemistry.[4]

Among the formaldehyde reactions, the reaction with hydroxyl (OH) radical is one of the most important ones. It is the main reaction pathway in formaldehyde oxidation,[5] and it is the key step in both ozone formation[2] and formaldehyde removal in cold molecular clouds[4].

There are two main channels for formaldehyde reaction with hydroxyl: (i) hydrogen abstraction to produce H_2O and HCO radical (this is the title reaction) and (ii) OH addition to generate the hydroxyl methoxy radical. The hydrogen abstraction reaction is the more favorable of these.[6] Xu et al.[5] reported that the addition channel has a higher barrier height than that for abstraction [5.7 kcal/mol vs. –1.0 kcal/mol by CCSD(T)/6-311+G(3df,2p)//CCSD/6-311++G(d,p)] and accounts for only 1% of the overall rate constant at T = 1000–1600 K based on variational transition state theory (VTST) calculations. (The reaction rate to produce HCOOH + H is also very small.[7]) Hence, in this work, we focus only on reaction (i). The reaction is assumed to involve bimolecular association to form a chemically activated hydrogen-bonded reaction complex (HCHO···HO) that can unimolecularly decompose into the final products, as follows:

$$\mathrm{HCHO + OH} \xrightarrow{1} \mathrm{HCHO\cdots HO} \xrightarrow{2} \mathrm{HCO + H_2O} \qquad (1)$$

where the first step is barrierless, and the transition state for the second step is denoted as TS. The first step is treated as reversible. Later in the article, the bimolecular reactant (HCHO + OH) is sometimes denoted as R, the hydrogen-bonded reaction complex (HCHO···HO) as RC, and the bimolecular product (HCO + H_2O) as P.

Kinetics of reaction (i) has been investigated experimentally in diverse temperature ranges.[4,8,9,10] In 2017, Ocaña et al.[4] observed abnormally high low-temperature rate coefficients by using the CRESU technique under ultralow temperature and pressure conditions (22-107 K, 0.05-2.37 mbar).

The rate constants of HCHO + OH reactions have been predicted theoretically[5,7,11,12,13,14] by using conventional transition state theory[11], variational transition state theory[13,14] (VTST), quasiclassical trajectories (QCT),[7] and ring polymer molecular dynamics (RPMD)[7]. Previous work[7] has emphasized the role of the reaction complex in the observed non-Arrhenius behavior at low temperature. Most theoretical studies[5,11,12,13] focus on temperatures above 200 K, but others, like the recent VTST study by de Souza Machado et al.[14] and the QCT/RPMD simulation by Mazo-Sevillano et al.[7], although they studied lower temperatures, failed to give consistent rate constants over the whole temperature range ($20 < T < 2200$ K)[14] and show large discrepancies compared to the experiment results[7].

The present study is carried out with a new version of the recently developed master equation program *TUMME*[15,16]. We employed the energy-resolved master equation[15,17,18,19,20,21,22,23,24,25,26,27,28] and obtained phenomenological rate constants from the master equation by the method of chemically significant eigenmodes (CSE theory[18,23,24,25,25,29]). Canonical variational theory[30] (CVT) with small-curvature tunneling[31] (SCT) is used for calculating the flux coefficients needed as input to the master equation. This allows us to include variational effects,[32] multidimensional tunneling,[33] and torsional anharmonicity[34] in the input flux coefficients.

2. Methodology

We distinguish the rate constant k from flux coefficients $\hat{k}$. The former is a time-independent phenomenological constant (at a given temperature and within the steady-state time frame) obtained from experiment or as output from the master equation or a mechanism, while the latter are measures of one-way reactive fluxes that are input to the master equation.

2.1 Master equation for the rate constants

As shown in eqn (1), there are two elementary reaction steps in the title reaction. We do not explicitly include a well-skipping reaction[35] in which R is converted directly to P. The energy E of the reaction complex is treated as a discrete variable on a grid. The size, ΔE, of each energy bin is set to 0.1 $k_{\mathrm{B}}T$ where k_{B} and T are is the Boltzmann constant and the temperature, and the highest energy $E_{\max}$ on the grid is set to 50 $k_{\mathrm{B}}T$ relative to the ground-state energy E_0 of reactant R. Bin η then contains energies from $E_{\max} - \eta\,\Delta E$ to $E_{\max} - (\eta-1)\,\Delta E$. The number of energy bins is denoted as N.

We assume that the back reaction of the bimolecular products, HCO and H_2O, is negligible so that their concentrations may be set equal to zero in the master equation. We also assume that the bimolecular reactants are fully thermalized.

The energy-resolved master equation for title reaction is then expressed as the following matrix equation:

$$\frac{\mathrm{d}\mathbf{y}}{\mathrm{d}t} = -\mathbf{W}\mathbf{y} + \mathbf{B}n_{\mathrm{HCHO}}n_{\mathrm{OH}}. \qquad (2)$$

where

- **y** is a concentration vector whose components y_η are the populations of the reaction complex in energy bin η, i.e., $y_\eta = y(E_\eta)$;
- **W** is a transition matrix for energy-relaxation and dissociation reactions of the reaction complex; it involves energy-relaxation probabilities $P(E_\eta|E_{\eta'})$ of the reaction complex

and microcanonical flux coefficients $\hat{k}(E_\eta)$ for the energy-selected dissociation of the complex;

- **B** is a transition vector containing microcanonical flux coefficients $\Delta\hat{k}(E_\eta)$ for the energy-selected association reaction into energy bin η.

In practice, we symmetrize eqn (2) to get a Hermitian transition matrix,

$$\frac{\mathrm{d}\tilde{\mathbf{y}}}{\mathrm{dt}} = -\mathbf{G}\tilde{\mathbf{y}} + \tilde{\mathbf{B}} n_{\mathrm{HCHO}} n_{\mathrm{OH}} \tag{3}$$

where a tilde denotes a vector that is left-multiplied by $\mathbf{F}^{-1}$, where **F** is a diagonal matrix whose elements are proportional to the square roots of the thermal populations of the RC[15], and **G** is the symmetrized transition matrix (given by $\mathbf{G} = \mathbf{F}^{-1}\mathbf{W}\mathbf{F}$) whose eigenpairs will be used to calculate rate constants. The main tasks to obtain rate constants are to construct **W** and **B** (or **G** and $\tilde{\mathbf{B}}$) and then solve the master equation.

2.2 Master equation for the time-dependent concentrations

The time-evolution for the present mechanism can only be obtained from the master equation if we introduce equations or assumptions to describe the evolution of reactant concentrations. In the previous versions (1.0–2.2) of *TUMME*, the time-evolution was calculated only under the assumption that all bimolecular pairs are treated as sinks; this is modeled by setting the concentrations of bimolecular pairs as zero, in which case reactants can only be unimolecular isomers. In order to solve for the time evolution when there are bimolecular reactants, version 3.0 of *TUMME*, which is introduced here, uses a pseudo-first-order assumption. In particular, we assume that **:**

a) the bimolecular product is a sink, i.e., terms corresponding to back reactions from products are neglected;
b) the forward bimolecular reaction is pseudo-first-order, i.e., HCHO is present in such large excess that its concentration n_{HCHO} can be taken as a constant. Then the time dependence of the OH concentration is given by

$$\frac{\mathrm{d}n_{\mathrm{OH}}}{\mathrm{d}t} = -\left[n_{\mathrm{HCHO}} \Sigma_{\eta=1}^{\mathrm{N}} \Delta\hat{k}_{\mathrm{R}\rightarrow\mathrm{RC}}(E_\eta)\right] n_{\mathrm{OH}} + \sum_{\eta=1}^{N} \hat{k}_{\mathrm{RC}\rightarrow\mathrm{R}}(E_\eta) y(E_\eta) \tag{4}$$

Combining eqn (4) with the nonhomogeneous eqn (2) yields a coupled set of homogeneous first-order ordinary differential equations with the extended concentration vector $\mathbf{y}^*$:

$$\frac{\mathrm{d}\mathbf{y}^*}{\mathrm{dt}} = -\mathbf{W}^*\mathbf{y}^* \tag{5}$$

where $\mathbf{y}^*$ is an extension of concentration vector **y**, and is obtained by adding n_{OH} as an

additional component of the vector **y:**

$$y_\eta^* = \begin{cases} y_\eta & 0 < \eta \le N \\ n_{\mathrm{OH}} & \eta = N+1 \end{cases} \tag{6}$$

where N is the number of energy bins in the concentration vector **y**, and $\mathbf{W}^*$ is an extension to the transition matrix **W**, in which association reactions involving the bimolecular reactant R are added (the dissociation reactions were already there). The elements of $\mathbf{W}^*$ are

$$W_{\eta\eta'}^* = \begin{cases} W_{\eta\eta'}; & 1 \le \eta \le N \text{ and } 1 \le \eta' \le N \\ -\Delta\widehat{k}_{\mathrm{R}\to\mathrm{RC}}(E_\eta) n_{\mathrm{HCHO}}; & 1 \le \eta \le N \text{ and } \eta' = N+1 \\ -\widehat{k}_{\mathrm{RC}\to\mathrm{R}}(E_\eta); & \eta = N+1 \text{ and } 1 \le \eta' \le N \\ n_{\mathrm{HCHO}} \Sigma_{\eta=1}^{\mathrm{N}} \Delta\widehat{k}_{\mathrm{R}\to\mathrm{RC}}(E_\eta); & \eta = \eta' = N+1 \end{cases} \tag{7}$$

We symmetrized the pseudo-first-order master equation (5) as

$$\frac{\mathrm{d}\tilde{\mathbf{y}}^*}{\mathrm{dt}} = -\mathbf{G}^*\tilde{\mathbf{y}}^* \tag{8}$$

where

$$\begin{aligned} \tilde{\mathbf{y}}^* &= \mathbf{F}^{*-1}\mathbf{y}^* \\ \mathbf{G}^* &= \mathbf{F}^{*-1}\mathbf{W}^*\mathbf{F}^* \end{aligned} \tag{9}$$

and where $\mathbf{F}^*$ is a diagonal matrix whose elements are

$$F_{\eta\eta}^* = \begin{cases} \sqrt{\rho_{\mathrm{RC}}(E_\eta) \exp(-\beta E_\eta)}; & 0 < \eta \le N \\ \sqrt{\dfrac{\Phi_{\mathrm{R}}^{\mathrm{rel}} Q_{\mathrm{R}}}{n_{\mathrm{HCHO}} \Delta E}}; & \eta = N+1 \end{cases} \tag{10}$$

The solution of eqn (5) is

$$\mathbf{y}^*(t) = \mathbf{F}^*\mathbf{U}^*\mathbf{E}^*\mathbf{U}^{*\mathsf{T}}\mathbf{F}^{*-1}\mathbf{y}_0^* \tag{11}$$

where $\mathbf{U}^*$ is the eigenvector matrix of symmetric transition matrix $\mathbf{G}^*$, $\mathbf{E}^*$ is a diagonal matrix with

$$E_{ii}^* = \mathrm{e}^{-L_i^* t} \tag{12}$$

where L_i^* is an eigenvalue of $\mathbf{G}^*$, and $\mathbf{y}_0^*$ is the initial condition. The superscript * is to distinguish notations with our previous *TUMME* article[15].

2.3 Input to the master equation

The energy-relaxation probabilities are modeled by the exponential-down model;[36] this model gives the following probability that a complex with energy between $E_{\eta'}$ and $E_{\eta'} + \Delta E$ before a collision with a bath gas will have an energy between E_η and $E_\eta + \Delta E$ after the collision:

$$P(E_\eta|E_{\eta'}) = A(E_{\eta'}) \exp\left(-\frac{E_{\eta'} - E_\eta}{\langle \Delta E_d \rangle}\right) \quad \text{for } E_{\eta'} > E_\eta \tag{13}$$

where $A(E_{\eta'})$ is a normlization constant. The energy transfer probabilities for $E_{\eta'} < E_\eta$ are obtained by the detailed balance. In eqn (13), $\langle \Delta E_d \rangle$ is the magnitude of the average energy transferred in collisions in which the complex loses energy.

Next we discuss the input microcanonical reactive flux coefficients.

a) RC → P Since both RC and TS are found to have only one conformer, we do not need multi-structural[37] transition state theory. Therefore, we calculate the microcanonical flux coefficients of RC→P by CVT/SCT as[15,30,31,37,38]

$$\hat{k}_{RC\to P}(E_\eta) = \frac{N_{RC,P}^{CVT/SCT}(E_\eta)}{h\rho_{RC}(E_\eta)} \tag{14a}$$

$$N_{RC,P}^{CVT/SCT}(E_\eta) \approx \frac{N_{RC,P}^{HO\text{-}CVT/SCT}(E_\eta)}{N_{RC,P}^{HO\text{-}‡/SCT}(E_\eta)} N_{RC,P}^{‡/SCT}(E_\eta) \tag{14b}$$

where $N_{RC,P}^{CVT/SCT}$is the anharmonic cumulative reactive probability calculated by CVT/SCT, h is Planck's constant; ρ_{RC} is the density of states of the reaction complex; ‡ and CVT denote the conventional transition state[39] (a dividing surface through the saddle point) and canonical variational transition state[30] (a dividing surface that maximizes the free energy of activation), respectively; and HO-‡/SCT and HO-CVT/SCT denote the harmonic oscillator approximation to anharmonic ‡/SCT and anharmonic CVT/SCT.

The density of states in eqn (14a) is evaluated as the inverse Laplace transform of the reaction-complex partition function Q_{RC}:

$$\rho_{RC}(E_\eta) = \frac{1}{2\pi i} \int_{\sigma-i\infty}^{\sigma+i\infty} Q_{RC}(\beta)\, e^{\beta E_\eta} d\beta \tag{15}$$

which is implemented in the *MSTor* program[40] by the steepest-descents method[41,42,43,44]. The harmonic approximation to the cumulative reactive probability is expressed as

$$N_{RC,P}^{HO\text{-}CVT/SCT}(E_\eta) = \int_{E_{0,RC}-V_a^{G*}}^{E_\eta - V_a^{G*}} d\varepsilon P_{RC,P}^{SCT}(\varepsilon) \rho_{RC,P}^{HO\text{-}CVT}(E_\eta - \varepsilon) \tag{16}$$

where $P_{RC,P}^{SCT}$ is the ground-state tunneling transmission probability evaluated by the small-curvature tunneling method; $\rho_{RC,P}^{HO\text{-}CVT}$ is the harmonic oscillator density of electronic-vibrational-rotational states of the canonical variational transition state between RC and P; $E_{0,RC}$ is the ground-state energy (with zero-point energy) of RC; V_a^{G*} is the adiabatic ground state potential energy of the canonical variational transition state; and ε is the energy in the reaction coordinate at the CVT.

Note that the right-hand side of eqn (16) depends on T because the location of the canonical variational transition state depends on T. Therefore the results of eqns (14a), (14b), and (16) depend parametrically on T; that is, we use a different set of values for each T.

We calculate $N_{\mathrm{RC,P}}^{\mathrm{HO\text{-}\ddagger/SCT}}$ and $N_{\mathrm{RC,P}}^{\ddagger/\mathrm{SCT}}$ by expressions analogous to eqn (16).

Note that $N_{\mathrm{RC,P}}^{\mathrm{CVT/SCT}}$, ρ_{RC}, $N_{\mathrm{RC,P}}^{\ddagger/\mathrm{SCT}}$, and Q_{RC} all contain anharmonicity in two ways: vibrational frequencies are scaled, and torsional anharmonicity is included (details of both are below).

b) R → RC The microcanonical flux coefficients of the barrierless association reaction R→RC are obtained by inverse Laplace transform of the canonical hard-sphere collision flux coefficient. The hard-sphere collision flux coefficient is

$$\hat{k}_{\mathrm{R\to RC}}(\beta) = \frac{\pi d_{\mathrm{R}}^2}{4}\sqrt{\frac{8}{\pi m_{\mathrm{R}}\beta}} \tag{17}$$

where β is $\frac{1}{\mathrm{k_B}T}$, and m_{R} and d_{R} are respectively the relative-translational reduced mass and the effective collision diameter of R. The canonical flux coefficient is the Laplace transform of the microcanonical flux coefficient and is given by

$$\hat{k}_{\mathrm{R\to RC}}(\beta) = \frac{1}{\Phi_{\mathrm{R}}^{\mathrm{rel}} Q_{\mathrm{R}}}\int \left[\hat{k}_{\mathrm{R\to RC}}(E)\rho_{\mathrm{R}}(E)\right]e^{-\beta E}dE \tag{18}$$

where ρ_{R}, $\Phi_{\mathrm{R}}^{\mathrm{rel}}$, and Q_{R} are respectively the joint density of states, the relative translational canonical partition function, and the electronic-vibrational-rotational canonical partition function of the bimolecular pair R; and the zero of energy is set at the ground state (including zero-point energy) of the reactant R. Taking the inverse Laplace transform yields[45]

$$\begin{aligned}\hat{k}_{\mathrm{R\to RC}}(E_\eta) &= \frac{1}{2\pi i}\int_{\sigma-i\infty}^{\sigma+i\infty}\hat{k}_{\mathrm{R\to RC}}(\beta)\Phi_{\mathrm{R}}^{\mathrm{rel}}Q_{\mathrm{R}}\,e^{\beta E_\eta}d\beta \\ &= \frac{8\pi d_{\mathrm{R}}^2}{h\rho_{\mathrm{R}}(E_\eta)}\left(\frac{\pi m_{\mathrm{R}}}{h^2}\right)\int_0^{E_\eta}\rho_{\mathrm{R}}(E_\eta-\varepsilon)\varepsilon d\varepsilon\end{aligned} \tag{19}$$

And the associated bin-selected microcanonical flux coefficient is

$$\begin{aligned}\Delta\hat{k}_{\mathrm{R\to RC}}(E_\eta) &= \hat{k}_{\mathrm{R\to RC}}(E_\eta)\frac{\rho_{\mathrm{R}}(E_\eta)e^{-\beta E_\eta}\Delta E}{\Phi_{\mathrm{R}}^{\mathrm{rel}}Q_{\mathrm{R}}} \\ &= \left[8\pi d_{\mathrm{R}}^2\left(\frac{\pi m_{\mathrm{R}}}{h^2}\right)\int_0^{E_\eta}\rho_{\mathrm{R}}(E_\eta-\varepsilon)\varepsilon d\varepsilon\right]\frac{e^{-\beta E_\eta}\Delta E}{h\Phi_{\mathrm{R}}^{\mathrm{rel}}Q_{\mathrm{R}}}\end{aligned} \tag{20}$$

where $\Delta\hat{k}_{\mathrm{R\to RC}}$ is the element of the vector **B**, and ΔE is energetic spacing of energy bins.

c) RC→R The microcanonical flux coefficients of the dissociation reaction RC→R, which

is the reverse reaction of the barrierless association reaction R→RC, are estimated by the detailed balance with R→RC, which yield[15],

$$\hat{k}_{\mathrm{RC}\to\mathrm{R}}(E_\eta) = \hat{k}_{\mathrm{R}\to\mathrm{RC}}(E_\eta) \times \frac{\rho_{\mathrm{R}}(E_\eta)}{\rho_{\mathrm{RC}}(E_\eta)} \tag{21}$$

$$= \left[8\pi d_{\mathrm{R}}^2 \left(\frac{\pi m_{\mathrm{R}}}{h^2}\right) \int_0^{E_\eta} \rho_{\mathrm{R}}(E_\eta - \varepsilon)\varepsilon d\varepsilon\right] \frac{1}{h\rho_{\mathrm{RC}}(E_\eta)}$$

2.4 Rate constants from solving the master equation

The phenomenological rate constants can be extracted by solving eqn (2) by interpreting the solution with CSE theory, which divides eigenvalues of the transition matrix into chemically significant eigenmodes and internal-energy-relaxation eigenmodes according to their magnitudes.[20,23,24,25,26] Let M be the total number of chemical configurations involved in the reaction system, let S be the number of chemical configurations included in the concentration vector (in the present case we have S equals 1 in Section 2.1, and it equals 2 in Section 2.2), and let N_{CSE} be the number of chemically significant eigenmodes. These variables are related by

$$N_{\mathrm{CSE}} = S - \delta_{MS} \tag{22}$$

where δ_{MS} is a Kronecker delta function that is 1 when M equals S (which is the case for a conservative system, i.e., a system without sinks) and 0 when M is greater than S (which is the case for a nonconservative system. i.e., a system with sinks, such that the concentration vector tends to the null vector when $t \to \infty$). In ref. 25, Miller and Klippenstein discussed a conservative reaction system where all chemical configurations (also called species in their article) are included in the concentration vector (denotes as $|w(t)\rangle$ in their article) and gave the relationship that N_{CSE} equals $S - 1$. The relationship in eqn (22) is a generalization of that result.

The chemically signficant eignemodes of **G** are used when extracting a rate constant or rate constants from the equations of section 2.1, while all the eigenmodes of $\mathbf{G}^*$ are used to derive the time evolution of the population from the equations of section 2.2. Because we assume the products are a nonreversible sink, the mechansim studied here is a nonconservative system; this means that N_{CSE} equals 1 for extracting rate constants from **G**.

Before one can obtain the rate constants, one must determine whether any of the chemical configurations have merged. As will be mentioned in Section 4.1, in the present reaction the reaction complex RC is only 3-4 kcal/mol lower than the reactant R, and – under some conditions of temperature and pressure – it can equilibrate with the reactant. When equilibrium is reached, R and RC should be "merged", i.e., considered as a single species.[15, 46] When a RC is merged with R, the title reaction becomes a one-step reaction between reactant R and product P that is bimolecular in both directions. (The rate constants involving RC, namely $k_{\mathrm{R}\to\mathrm{RC}}$, $k_{\mathrm{RC}\to\mathrm{R}}$, and $k_{\mathrm{RC}\to\mathrm{P}}$, become meaningless.)

The product P is assumed to be a sink in our treatment, and thus our master equation calculations do not not give phenomenological rate constants of reactions starting from the product.

When R and RC have not merged, four rate constants $k_{\mathrm{R}\to\mathrm{RC}}$, $k_{\mathrm{R}\to\mathrm{P}}$, $k_{\mathrm{RC}\to\mathrm{R}}$, and $k_{\mathrm{RC}\to\mathrm{P}}$ are obtained from the chemically significant eigenvector by eqns (47) of ref. 15. Specifically, for the master equation we studied here, eqn (3), because we have N_{CSE} equal to 1, the expression of $k_{\mathrm{RC}\to\mathrm{R}}$ becomes

$$k_{\mathrm{RC}\to\mathrm{R}} = \sum_{\eta=1}^{N} \hat{k}_{\mathrm{RC}\to\mathrm{R}}(E_\eta) \frac{u_\eta^{(1)} F_\eta}{\Sigma_{\eta=1}^{N} u_\eta^{(1)} F_\eta} \tag{23}$$

where $u_\eta^{(1)}$ is an element of the eigenvector of **G** that corresponds to the chemically significant eigenvalue (which is L_1), and F_η is an element of the diagonal matrix **F**. The expression for $k_{\mathrm{RC}\to\mathrm{P}}$ and $k_{\mathrm{R}\to\mathrm{RC}}$ is the same except $\hat{k}_{\mathrm{RC}\to\mathrm{P}}(E_\eta)$ replaces $\hat{k}_{\mathrm{RC}\to\mathrm{R}}(E_\eta)$ and $\Delta\hat{k}_{\mathrm{R}\to\mathrm{RC}}(E_\eta)$ replaces $\hat{k}_{\mathrm{RC}\to\mathrm{R}}(E_\eta)$, respectively. Note that eqn (23) is equivalent to eqn (5) of an earlier article.[47] For $k_{\mathrm{R}\to\mathrm{P}}$, eqns (47) of ref. 15 reduce for our case to:

$$k_{\mathrm{R}\to\mathrm{P}} = \sum_{\eta'=1}^{N} \sum_{\eta=1}^{N} \hat{k}_{\mathrm{RC}\to\mathrm{P}}(E_{\eta'}) \, (\mathbf{W}^{-1})_{\eta'\eta} \, \Delta\hat{k}_{\mathrm{R}\to\mathrm{RC}}(E_\eta) \tag{24}$$

$$- \sum_{\eta'=1}^{N} \sum_{\eta=1}^{N} \hat{k}_{\mathrm{RC}\to\mathrm{P}}(E_{\eta'}) \frac{F_{\eta'} u_{\eta'}^{(1)} F_\eta^{-1} u_\eta^{(1)}}{L_1} \Delta\hat{k}_{\mathrm{R}\to\mathrm{RC}}(E_\eta)$$

In ref. 15, the bimolecular-to-bimolecular rate constant is written as a sum over relaxational eigenmodes, but here we write it equivalently as a sum over all modes minus the contribution of the chemically significant eigenmode.

In the present mechanism, when the reaction complex is merged with the reactant, there is no CSE eigenmode. If we label the merged R and RC as R, we have only one rate constant, $k_{\mathrm{R}\to\mathrm{P}}$, and it is given by

$$k_{\mathrm{R}\to\mathrm{P}} = \sum_{\eta'=1}^{N} \sum_{\eta=1}^{N} \hat{k}_{\mathrm{RC}\to\mathrm{P}}(E_{\eta'}) \, (\mathbf{W}^{-1})_{\eta'\eta} \, \Delta\hat{k}_{\mathrm{R}\to\mathrm{RC}}(E_\eta) \tag{25}$$

While the collision rate (also pressure, embedded in **W**) approaches zero, eqn (25) degenerates to eqn (10b) of ref 25.

Even though rate constants are calculated from the version of the master equation that does not involve the pseudo-first-order assumption, the time evoution curves produced by rate constants match perfectly well with those from eqn (11) which is derived using the pseudo-first order assumption. This is illustrated in Figure S3 in the supporting information.

Rate constants should satisfy the macroscopic detailed balance condition. Georgievskii et al. concluded that as long as CSE assumptions are good, the phenomenological rate constants extracted from master equations satisfy this condition[26]. Therefore $k_{\mathrm{R}\to\mathrm{RC}}$ and $k_{\mathrm{RC}\to\mathrm{R}}$are not independent, and their ratio should equal the equilibrium constant. The ratios of these two rate constants at various pressures and temperatures are listed in Tables S1 and S2 of Supporting Information, and these tables confirm that detailed balance is well satisfied when the CSE assumptions are well satisfied.

3. Computational details

Based on optimized geometries by the CCSD(T)/aug-cc-pVTZ method from Ali et al.'s work[12], we calculated the T_1 diagnostics[48,49] for reactants, reaction complex, transition state, and products of the title reaction with the CCSD[50]/ jul-cc-pVTZ[51,52] method. Table 1 shows that all obtained T_1 values are smaller than 0.045 for radicals and 0.02 for closed-shell molecules, indicating that all the species involved in the title reaction can be well approximated by a single-configuration reference wave function. This is consistent with the finding of Machado et al.[14] Therefore our direct dynamics calculations used single-configuration Kohn-Sham theory with the M08-HX[53] exchange-correlation functional, which has shown good performance in calculating transition structures[54], bond dissociation enthalpies[55] and barrier heights[56] for systems well characterized by a single electronic configuration.

Table 1. T_1 diagnostics

Singlet species	T_1	Radical species	T_1
Formaldehyde	0.015	OH	0.008
H_2O	0.009	Reaction Complex	0.014
		Transition State	0.032
		HCO	0.026

The M08-HX exchange-correlation functional method combined with aug-cc-pVTZ[57] basis set (the combination is denoted M08-HX/aug-cc-pVTZ) was used to obtain the potential energy surface (PES) of the reaction for the dynamic calculations. The M08-HX/aug-cc-pVTZ frequencies are scaled by 0.975[58] to include anharmonicity and to compensate for systematic errors in M08-HX/aug-cc-pVTZ.

We use enthalpies of reaction at 0 K and enthalpies of activation at 0 K as a way to compare various theoretical electronic structure methods and to illustrate reaction profiles. Enthalpies of a species (reactant, product, or transition state) at 0 K are equal to that species' equilibrium Born-Oppenheimer potential energy plus its zero-point vibrational energy; relative enthalpies are obtained by subtracting the enthalpy of the reactant, and the relative enthalpy of a transition state is called the enthalpy of activation.

To examine the accuracy of the M08-HX/aug-cc-pVTZ model chemistry, we compared the relative enthalpies of stationary points along the PES (reactant, reaction complex, transition states, and product) to those computed by high-level coupled cluster calculations, in particular CCSD(T)-F12b[59,60] /jul-cc-pVTZ calculations. For these coupled cluster calculations, we used the CCSD(T)/aug-cc-pVTZ optimized geometries and frequencies reported by M. Akbar Ali et al[12]. Density functional calculations were carried out using *Gaussian 16*[61], and coupled cluster calculations were performed using *Molpro 2015*[62].

In the direct dynamic calculations, the minimum-energy path between RC and P was obtained with a step size of 0.002 Å (with all coordinates scaled to a mass of 1 amu) by *Gaussrate 17*[63], and the Hessian was calculated at each step. The small-curvature tunneling transmission

possibility $P_{\mathrm{RC,P}}^{\mathrm{SCT}}$ is calculated by *Polyrate 2017*[64]. The density of states including torsional anharmonicity is evaluated by *MSTor*[40]. The computational details of the torsional anharmonicity of the RC and the saddle point are given in the SI.

The bath gas considered in this article is N_2. The collision rate between the RC and the bath gas is calculated by the Lennard-Jones (LJ) model. The LJ parameters ε, σ for N_2 and RC are 56.993 cm^{-1}, 191.134 cm^{-1} and 3.74 Å, 4.94 Å respectively[12]. The energy-transfer-down parameter $\langle \Delta E_{\mathrm{d}} \rangle$ is taken as $200(T/300)^{0.85}$ cm^{-1}.[12]

The hard-sphere model is used for collisions of bimolecular reactants. To obtain the average collision diameter d_{R} in eqn (17), we first substituted each atom in the molecule by a sphere with radius equal to the collision radius[65] of the atom. Then we chose the length of the model along the O-C direction as the collision diameter for HCHO and the length along the O-H direction as collision diameter for OH radical. This yields 4.515 Å and 3.704 Å, respectively, and we used their arithmetic average for d_{R}.

The master equation is solved by *TUMME*–version 3.0[16] in quadruple precision.

Since we study the reaction under pseudo-first-order conditions with the concentration of HCHO in excess, the partial pressure of HCHO should be much larger than that of OH, but because we assume all energy transfer collisions are with the bath gas, it should be much smaller than that of N_2. In the present work, we calculated the time evolution from eqn (11) for $T = 100$ K and $p = 10$, 10^4, and 10^7 Torr. According to the ideal gas equation, the corresponding concentrations of N_2 are 1.6×10^{-2}, 1.6, and 1.6×10^3 mol/L. The pseudo-first order master equation [eqn (5) or (8)] is homogenous; and therefore the concentration of OH is arbitrary as long as it is much less than that of HCHO, and the concentration of HCHO is arbitrary as long as it is much less than that of N_2. For concreteness and in order to use concentration units in the examples, we arbitrarily assigned the initial concentration of OH as 10^{-7} mol/L and the essentially constant concentration of HCHO as 10^{-5} mol/L. In all cases when we specify a pressure, we mean the pressure of N_2, which, accordingly to the above discussion, is essentially the same as the total pressure.

4. Results and discussion

4.1 Energies and structures

The geometries of the reaction complex (RC) and transition state (TS) by the M08-HX/aug-cc-pVTZ method are presented in Figure 1. As the figure shows, the reaction complex RC is a hydrogen-bonding-stabilized van der Waals complex (HCHO···HO). To form transition structure (OHCH···OH) from the RC, the OH radical needs to reorient for abstracting the hydrogen of HCHO.

The enthalpy profile calculated for the title reaction by the M08-HX/aug-cc-pVTZ method is shown in Figure 2. For comparison, the results by CCSD(T)-F12b/jul-cc-pVTZ//CCSD(T)/aug-cc-pVTZ calculations are also given in Figure 2. From the values in the figure, one can calculate

that the M08-HX results have a mean unsigned deviation of 0.49 kcal/mol from the coupled cluster benchmark for the enthalpies of the complex, the transition state, and the products relative to the reactants.

Figure 2 shows that the enthalpy of the complex RC is 3–4 kcal/mol lower than that of the reactant R; this indicates a medium-strength hydrogen-bonding interaction, and the transition state is also slightly lower than R.

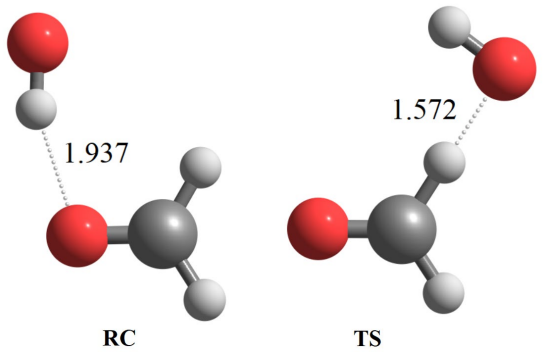

Figure 1. The geometry structures of RC and TS optimized by M08-HX/aug-cc-pVTZ. Distances are shown in Å.

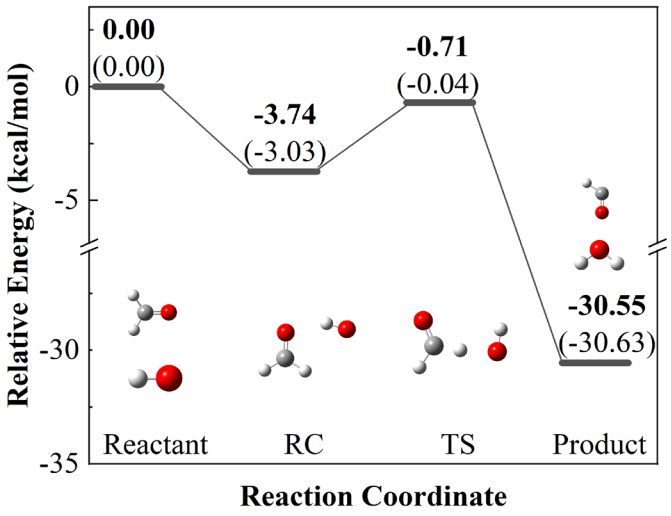

Figure 2. M08-HX/aug-cc-pVTZ enthalpies and enthalpies of activation at 0 K relative to the reactants. The enthalpy at 0 K equals the electronic energy plus the zero-point energy. The values in parentheses are benchmarks calculated by CCSD(T)-F12b/jul-cc-pVTZ//CCSD(T)/aug-cc-pVTZ with zero-point energies estimated by CCSD(T)/aug-cc-pVTZ. The optimization and frequency calculations for CCSD(T)/aug-cc-pVTZ are from ref. 12.

4.2 Rate constants

The CSE theory[15,25,26], assumes that there are will be N_{CSE} eigenvalues much smaller than others. As explained in Section 2.4, in the present case N_{CSE} is 1 below the merger temperature and 0 above it. Therefore, below the merger temperature, the rate constants are computed from

one eigenpair of the transition matrix **G**. Table 2 shows, for various combinations of T and p, the two smallest eigenvalues (the chemically significant eigenvalue and the slowest internal-energy-relaxation eigenvalue) of **G**. We can see that there is a good separation of time scales at 100 K and for high enough p at 300–600 K, but not in the other cases.

Table 2. The smallest two eigenvalues of transition matrix **G** [a]

p/Torr	10^{-2}		10^{1}		10^{4}		10^{7}	
T/K	$\frac{L_1}{Z}$	$\frac{L_2}{Z}$	$\frac{L_1}{Z}$	$\frac{L_2}{Z}$	$\frac{L_1}{Z}$	$\frac{L_2}{Z}$	$\frac{L_1}{Z}$	$\frac{L_2}{Z}$
100	2.95×10^{-4}	0.14	2.84×10^{-5}	0.12	6.70×10^{-7}	0.10	3.22×10^{-9}	9.66×10^{-2}
300	0.12	0.60	6.12×10^{-2}	0.45	2.13×10^{-2}	0.29	3.76×10^{-3}	0.15
600	0.65	0.99	0.45	0.93	0.25	0.77	8.96×10^{-2}	0.48
1000	1.00	1.00[b]	1.00	1.00[b]	0.80	1.00[b]	0.40	0.92

[a] L_1 and L_2 denote the smallest and second smallest eigenvalue of **G**; Z denotes the collision frequency calculated by the LJ model [eqn (48) of ref 15].

[b] These values are calculated with $\Delta E = 0.01k_{\mathrm{B}}T$; others are calculated with $\Delta E = 0.1k_{\mathrm{B}}T$. We found that at high temperature, the second smallest eigenvalue is sometimes sensitive to the energy step ΔE.

Rather than determine when to merge R and RC from the ratio of eigenvalues in Table 2, we can employ the projection of the chemically significant eigenvector onto the internal-energy-relaxation space as the criterion to monitor mergers; the projection is defined as[15, 26]

$$P = 1 - EPCS \tag{26}$$

where *EPCS* denotes the squared projection of the chemically significant eigenvector onto the basis vector of the chemical space [eqn (79) of ref 15]. Here the chemical space basis vector corresponds to a Boltzmann distribution of the bins of RC. We set the threshold to be 0.2, and when value of the projection P is greater than 0.2, the RC is considered to be thermally equilibrated with R. Values of the projection P calculated at different pressures are plotted as functions of temperature in Figure 3. For a specific pressure, we can find a merger temperature T_{m}, above which R and RC are merged. With the merger condition taken as $P = 0.2$, T_{m} equals about 200, 250, 300, and 450 K for pressures of 10^{-2}, 10, 10^4, and 10^7 Torr, respectively. Table 2 and Figure 3 both show that mergers are favored by high temperature and low pressure. In fact, the figure is consistent with Table 2 if we put the merger boundary at $\frac{L_2}{L_1}$ equal to 4. We list some values of the resulting rate constants in Tables 3 and 4, where they are compared with flux coefficients.

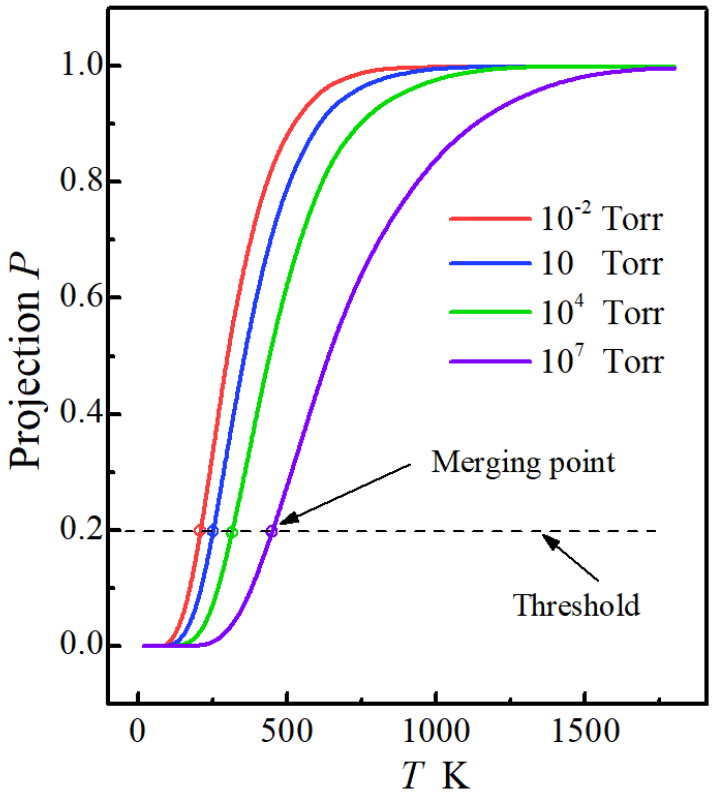

Figure 3. Projection of the chemical significant eigenvector onto the internal-energy-relaxation space.

Table 3. Logarithms (base 10) of rate constants and flux coefficients (in cm^3 $molecule^{-1}$ s^{-1})

T(K)/p(Torr)	$k_{R\rightarrow RC}$ 10^{-2}	$k_{R\rightarrow RC}$ 10^{1}	$k_{R\rightarrow RC}$ 10^{4}	$k_{R\rightarrow RC}$ 10^{7}	$\hat{k}_{R\rightarrow RC}$ HPL[a]	$k_{R\rightarrow P}$ 10^{-2}	$k_{R\rightarrow P}$ 10^{1}	$k_{R\rightarrow P}$ 10^{4}	$k_{R\rightarrow P}$ 10^{7}
20	-23.62	-17.25	-10.15	-9.99	-9.99	-10.08	-10.08	-10.58	-13.45
100	-19.71	-15.34	-10.90	-9.67	-9.63	-10.58	-10.58	-10.61	-11.96
200	-19.35	-15.64	-11.76	-9.71	-9.48	-10.88	-10.87	-10.88	-11.34
250		-15.77	-12.05	-9.79	-9.43		-10.97	-10.97	-11.26
300			-12.29	-9.87	-9.39		-10.97	-10.97	-11.17
450				-10.06	-9.30		-10.90	-10.90	-10.98
600					-9.24		-10.83	-10.83	-10.87
1000					-9.13		-10.56	-10.56	-10.56

[a] HPL denotes the high-pressure limit which is the canonical flux coefficient[25]. In our model, the flux coefficient is zero for R→P.

Table 4. Logarithms (base 10) of rate constants and flux coeffieiencts (in s^{-1})

T(K)/p(Torr)	$k_{RC\to R}$ 10^{-2}	$k_{RC\to R}$ 10^{1}	$k_{RC\to R}$ 10^{4}	$k_{RC\to R}$ 10^{7}	$\hat{k}_{RC\to R}$ HPL[a]	$k_{RC\to P}$ 10^{-2}	$k_{RC\to P}$ 10^{1}	$k_{RC\to P}$ 10^{4}	$k_{RC\to P}$ 10^{7}	$\hat{k}_{RC\to P}$ HPL[a]
20	-42.36	-35.99	-28.88	-28.73	-28.73	-4.67	-4.67	-4.67	-4.67	-4.67
100	-4.16	0.20	4.65	5.88	5.91	1.99	3.97	5.24	5.48	5.48
200	0.80	4.47	8.31	10.36	10.59	3.68	6.25	8.17	9.11	9.27
250		5.28	8.94	11.17	11.53		6.63	8.58	9.75	10.03
300			9.33	11.69	12.15			8.86	10.19	10.60
450				12.47	13.13				10.85	11.54

[a]HPL denotes the high-pressure limit which is the canonical flux coefficient[25].

For the four pressures in Table 2 and Figure 3 and for temperature ranges in which the merger does not occur, Figures 4 shows R→RC and R→P phenomenological rate constants extracted from eqn (2). Figure 4 reveals that $k_{R\to RC}$ and $k_{R\to P}$ show very different dependences on pressures. As pressure increases, $k_{R\to RC}$ increases, whereas $k_{R\to P}$ decreases. At high p and low T, energetic molecules coming from the reactant will tend to be stabilized in the reaction complex RC rather than proceeding straight to products, and thus the rate constant $k_{R\to P}$ is small under those conditions. Note that although we do not include an R → P elementary step, we still get reactions producing P. This occurs in two ways: (A) Molecules may access RC-like geometries (so that they may be considered to be metastable RC species) and react to form P before they are stabilized. (B) Reaction may occur by tunneling from stabilized RC or by overbarrier processes from the high-energy tail of stabilized RC. (All the high-energy bins of RC correspond to metastable RC). Low pressure and high temperature are favorable for conversion to product before stabilization (route A) and are also – as we have seen – favorable for equilibration of RC with reactants. Because of routes A and B, it is unnecessary to include an elementary R → P step unless one identifies a path from R to P that does not pass through geometries that can be considered to belong to excited vibrational states of RC. And if one did include an elementary R → P step, it would entail double counting some trajectories unless one reduced the probability of R → RC to eliminate those RC that pass rapidly to product.

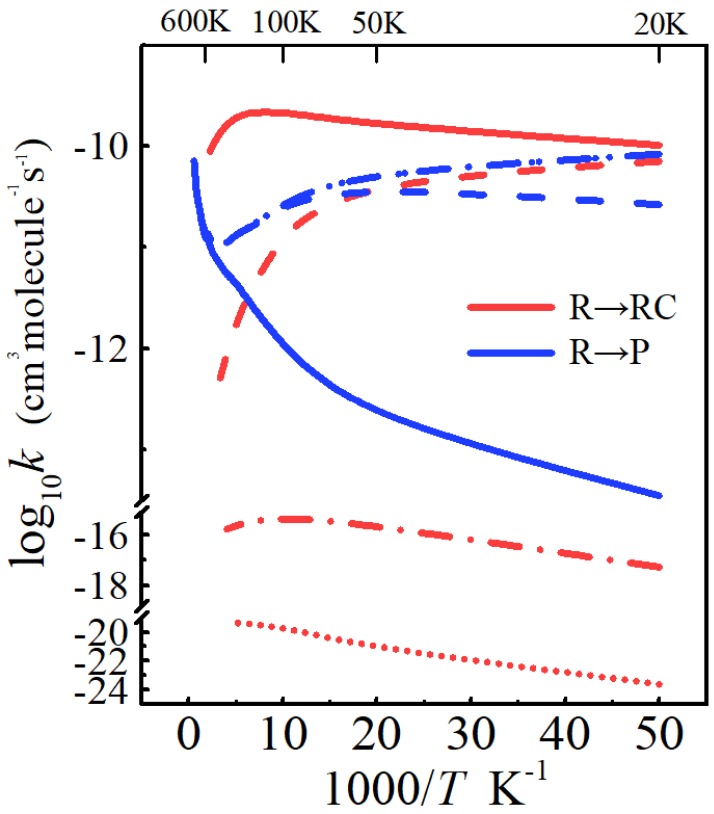

Figure 4 Phenomenological bimolecular rate constants for R→RC and R→P extracted from the master equation by CSE theory. Solid lines for 10^7 Torr; dashed lines for 10^4 Torr; dash-dot lines for 10 Torr; dotted lines for 10^{-2} Torr. This figure includes only unmerged (*T*,*p*) conditions (using the $P = 0.2$ criterion).

For the four pressures in Table 2 and Figures 3 and 4 and for temperature ranges in which the merger does not occur, Figure 5 shows the $k_{RC\rightarrow R}$ and $k_{RC\rightarrow P}$, phenomenological rate constants extracted from eqn (2). The figure shows that that $k_{RC\rightarrow R}$ is more sensitive to pressure than $k_{RC\rightarrow P}$, and at low temperatures $k_{RC\rightarrow P}$ is much larger than $k_{RC\rightarrow R}$ due to the lower barrier and the tunneling between the reaction complex and the product.

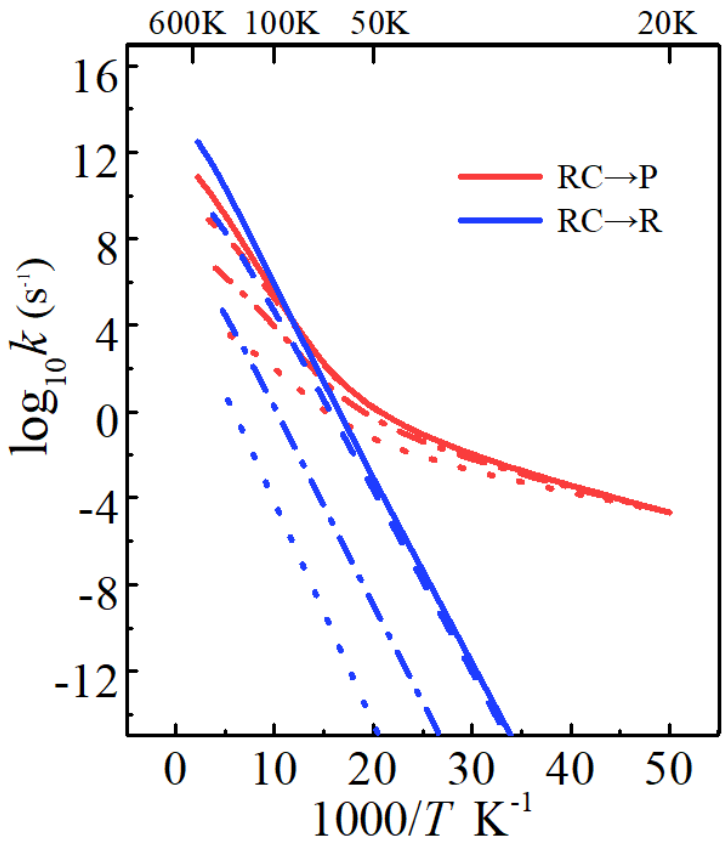

Figure 5 Phenomenological bimolecular rate constants for RC→R and RC→P extracted from the master equation by CSE theory. Solid lines for 10^7 Torr; dashed lines for 10^4 Torr; dash-dot lines for 10 Torr; dotted lines for 10^{-2} Torr. This figure includes only unmerged (*T*,*p*) conditions (using the $P = 0.2$ criterion).

4.3 Role of the reaction complex

In previous work on the high-pressure and low-pressure limits of the CH_3OH + OH abstraction reaction[66], it was found that high pressures stabilize an intermediate complex and that tunneling will speed up the depletion of that complex at low temperature. Here we use the master equation to quantitatively assess the corresponding issues for the HCHO + OH reaction.

For a temperature of 100 K and pressures of 10 Torr, 10^4 Torr, and 10^7 Torr, Figure 6 shows the depletion of OH radical and the buildup and depletion of the reaction complex, where the time evolution of their concentrations is obtained from the solution of eqn (11). The initial concentration of OH is taken as 10^{-7} mol/L; the concentrations of HCHO considered to be constant at 10^{-5} mol/L; the initial concentration of RC is zero; and the constant concentrations of bath gas are specified in Section 3. Figure 6 shows that the reaction complex RC only accumulates to a significant extent at high pressures.

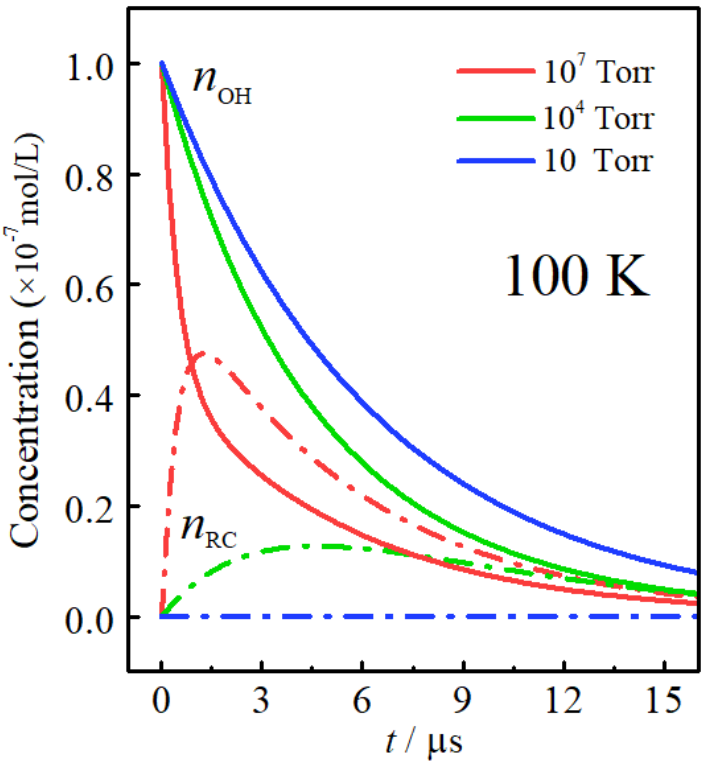

Figure 6. The time-evolution of n_{OH} (solid lines) and n_{RC} (dash-dot lines) evaluated by eqn (11). The initial condition is set as $n_{OH}(t = 0) = 10^{-7}$ mol/L, $n_{RC}(t = 0) = 0$ and n_{HCHO} is assumed to be constant at 10^{-5} mol/L.

To further explore the dependence of the time evolution profiles on pressure and tunneling, we consider the time-dependent unitless quantity defined as

$$f(t) = \frac{\sum_{E_\eta \le E_0^\ddagger} y_{RC}(E_\eta, t)}{n_{OH}(t = 0)} \tag{27}$$

where $E_0^{\ddagger}$ is the ground-state enthalpy of the conventional transition state between RC and P. When the zero of energy is at the reactant ground state, as it is in the present article, the ground-state enthalpy of the conventional transition state is the conventional-transition-state-theory approximation to the ground-state vibrationally adiabatic barrier height. The fraction defined in eqn (27) may be interpreted as the fraction of OH radicals that have been converted to stabilized RC. For several pressures (10, 100, 10^3, and 10^7 Torr) and a temperature of 100 K, Figure 7 compares the calculated f(t) with and without including RC→P tunneling in the master equation calculations.

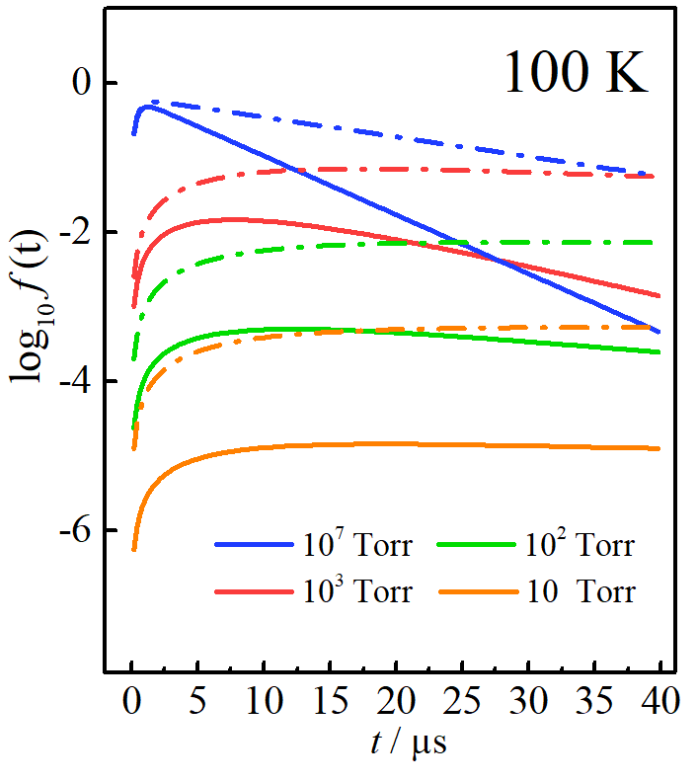

Figure 7. Time evolution of the OH radicals that have been converted to stabilized RC. Solid lines denote results that include RC→P tunneling while dash-dot lines denote results without RC→P tunneling. The abscissa is the time after initiation of the reaction.

Since the ground-state energy ($E_0^{\ddagger}$) of the RC–P transition state is lower than that of the reactant R, and since P is treated as a sink, there is only one way to accumulate complexes, and that is by deactivation of energetic RC by collisions with bath gas molecules. The collision rate is proportional to pressure, and thus – for a given time after initiation– we expect $f(t)$ to be larger when the pressure is higher; Figure 7 shows this expected trend. It also shows that, when tunneling is included, that the fraction f(t) reaches its maximum within a few μs (<5 μs), and then stays in a plateau close to the maximum for a time period > 40 μs at 10 Torr, ~20 μs at 100 Torr, ~10 μs at 10^3 Torr, and ~2 μs at 10^7 Torr. This behavior is a result of competing effects since high pressure both increases deactivation of energetic RC and increases the activation of stabilized

RC. Figure 7 shows that the concentration vs. time profile of RC is quite different when tunneling is excluded. Without tunneling, the fraction $f(t)$ shows a much slower decay.

4.4 Experimentally observable rate constants

Rate constants for pseudo-first-order radical reactions are usually extracted from experiment by modeling the reaction as

$$\frac{\mathrm{d}n_{\mathrm{OH}}}{\mathrm{d}t} = -k_{\mathrm{exp}}\, n_{\mathrm{HCHO}} n_{\mathrm{OH}} \tag{28}$$

with n_{HCHO} constant. This yields

$$n_{\mathrm{OH}}(t) = n_{\mathrm{OH}}(t=0)\exp(-k_{\mathrm{exp}} n_{\mathrm{HCHO}} t) \tag{**Error! Bookmark not defined.**29}$$

where k_{exp} is usually taken as the "rate constant", but actually it is not[25]. The next question to explore is: What is the relationship of k_{exp} to the rate constants calculated from the master equation?

We start with the phenomenological kinetic equations containing the four rate constants from solution of the master equation:

$$\frac{\mathrm{d}n_{\mathrm{OH}}}{\mathrm{d}t} = -(k_{\mathrm{R\to RC}} + k_{\mathrm{R\to P}}) n_{\mathrm{HCHO}} n_{\mathrm{OH}} + k_{\mathrm{RC\to R}} n_{\mathrm{RC}} \tag{30}$$

$$\frac{\mathrm{d}n_{\mathrm{RC}}}{\mathrm{d}t} = -(k_{\mathrm{RC\to R}} + k_{\mathrm{RC\to P}}) n_{\mathrm{RC}} + k_{\mathrm{R\to RC}} n_{\mathrm{HCHO}} n_{\mathrm{OH}} \tag{31}$$

The next step depends on whether the reaction complex and the bimolecular reactant are merged.

4.4.1 When R and RC are merged

For temperatures above T_m, a merger has occurred, the concentration of RC no longer appears (it is merged into the concentration of R), and the eqns (31) and (30) degenerate to

$$\frac{\mathrm{d}n_{\mathrm{OH}}}{\mathrm{d}t} = -k_{\mathrm{R\to P}} n_{\mathrm{HCHO}} n_{\mathrm{OH}} \tag{32}$$

Comparing this to eqn (28) then yields

$$k_{\mathrm{exp}} = k_{\mathrm{R\to P}} \tag{**Error! Bookmark not defined.**33}$$

where $k_{\mathrm{R\to P}}$ is calculated by eqn (25). Figure 8 shows the rate constant $k_{\mathrm{R\to P}}$ at $T > T_{\mathrm{m}}$. Figure 4 confirms the pressure dependence of $k_{\mathrm{R\to P}}$ at low temperatures, while Figure 8 shows that pressure barely affects $k_{\mathrm{R\to P}}$ at $T > T_{\mathrm{m}}$. The pressure independency at high T can be interpreted as a result of chemical equilibration of R with RC and thermal equilibration of the energy bins of RC. Our results match well with the experiments of Zabarnick et al.[8], who studied T between 292 and 597 K and p between 35 and 300 Torr and the experiments of Sivakumaran et al.[9], who studied T between 202 and 399 K and p at 50 Torr and 100 Torr. However, for $T > 1000$ K, our calculation gives larger rate constants than those of Vasudevan et al.[10], who studied the reaction at a pressure of 1216 Torr, by a factor of 1.5 at 1000 K and 1.8 at 1670 K.

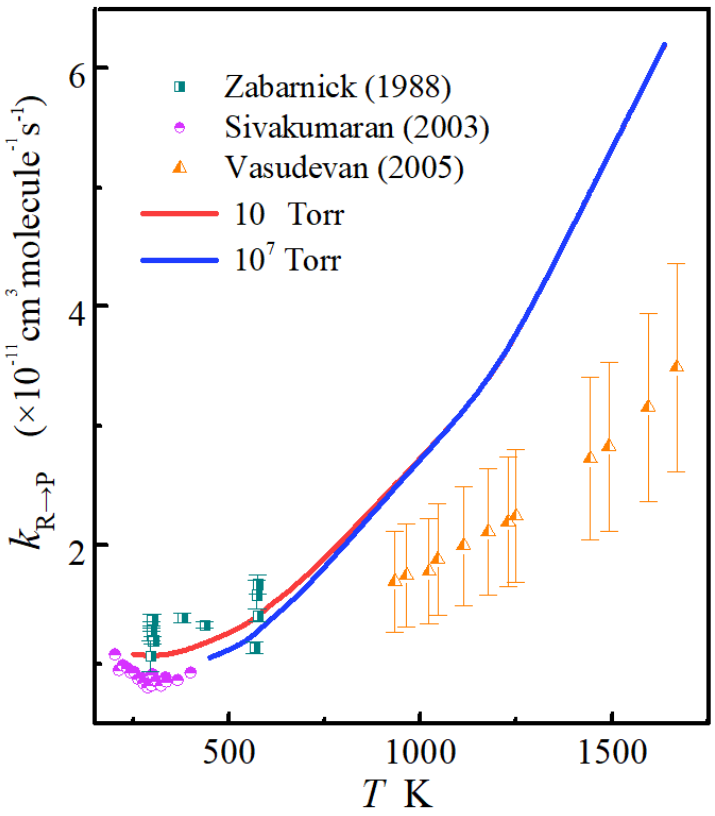

Figure 8. Comparison of theoretical rate constants calculated above the merger temperatures to the experimentally observed rate constants. Two pressures are shown for the theoretical rate constants; the lowest temperature for each pressure is the merger temperature for that pressure (using the $P = 0.2$ criterion), which is 250 K for 10 torr and 450 K for 10^7 Torr. Values of $k_{R\to P}$ at all pressures from 10^{-2} to 10^7 Torr would agree within plotting accuracy at $T > 1000$ K. Rate constants for $p < 10$ Torr are omitted in this figure since they overlap with the curve for 10 Torr. Data for $p = 10^2$ Torr are not shown because they agree (within plotting accuracy) with the rate constants at 10 Torr all the way down to the merger temperature, which is 300 K for 10^2 Torr.

4.4.2 When R and RC are not merged

For temperatures below the merger, we have four rate constants, and we must consider how to compare to experimental results obtained by eqn (28). In order to get the experimentally observed rate constant, we need derive an approximate expression like eqn (28) from the phenomenological mechanistic eqns (30) and (31). We can do this in two possible ways:

(a) Neglect the reverse reaction from RC. At the very first stage of reaction, the concentration of the reaction complex can be neglected, and we obtain

$$k_{\text{exp}}^{\text{f}} = k_{R\to RC} + k_{R\to P} \tag{34}$$

where the superscript "f" denotes that only forward reactions are considered here.

(b) Make the steady-state approximation (SSA) to RC. When the pressure is increased, the reverse reaction from RC to R become significant. The SSA provides a way to consider the reverse reaction. Applying the SSA to eqns (30) and (31) in the usual way[67] yields

$$k_{\mathrm{exp}}^{\mathrm{SSA}} = \frac{k_{\mathrm{R}\to\mathrm{RC}} k_{\mathrm{RC}\to\mathrm{P}}}{k_{\mathrm{RC}\to\mathrm{R}} + k_{\mathrm{RC}\to\mathrm{P}}} + k_{\mathrm{R}\to\mathrm{P}} \tag{35}$$

The $k_{\mathrm{R}\to\mathrm{P}}$ in eqn (34) and (35) is calculated from eqn (24). Both ways (methods (a) and (b)) to produce an experimentally observable rate constant for $T < T_{\mathrm{m}}$ are shown in Figure 9, where they are compared to experiments of Ocaña et al., who found no effect of pressure in their experiments at low temperatures [4]. Pressures investigated in their work range from ~0.04 Torr to ~2 Torr, which is consistent with our finding of no pressure effect in this pressure range. However, at higher pressures, both methods of extracting rate constants from the master equation for $T < T_{\mathrm{m}}$ show significant pressure dependence. Although we estimated the capture process for the bimolecular reactant by the simple hard-sphere model, the results show remarkably good agreement with experiments. In particular, on average the experimental data points in Figure 9 agree with our calculated low-pressure limit within about 30%, which is comparable to the experimental scatter.

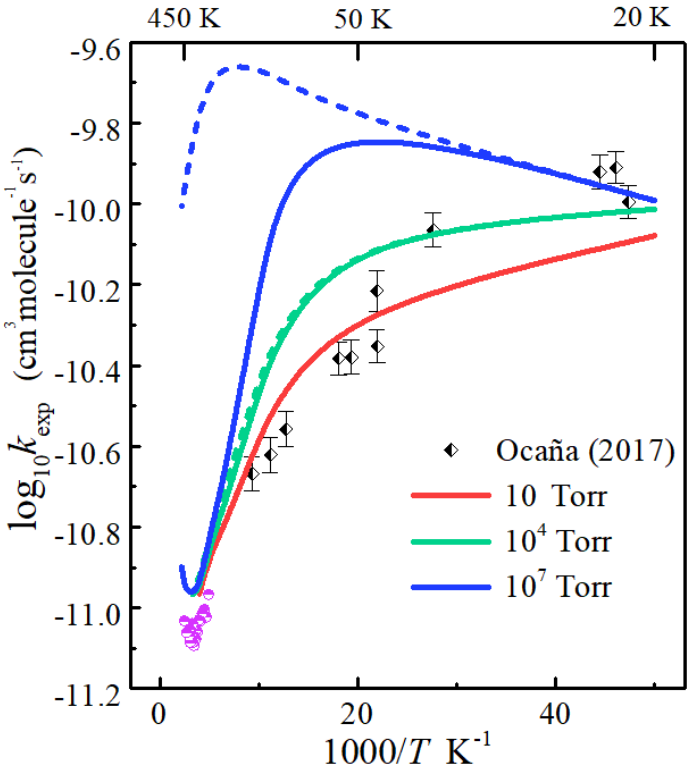

Figure 9. The experimentally observed constants. Solid lines denote $k_{\mathrm{exp}}^{\mathrm{SSA}}$ and dashed lines denote $k_{\mathrm{exp}}^{\mathrm{f}}$. Note $k_{\mathrm{exp}}^{\mathrm{f}}(p = 10\ \mathrm{Torr})$ and $k_{\mathrm{exp}}^{\mathrm{SSA}}(p = 10\ \mathrm{Torr})$ are overlapped. Data for $p < 10$ Torr for both methods are omitted from this figure since they overlap with the curves for 10 Torr.

Does either eqn (34) or (35) reproduce the decay curve of OH radical? To answer this question, Figure 10 compares the time-evolution of n_{HCHO} at 100 K using the predicted experimentally observable constant $k_{\mathrm{exp}}^{\mathrm{f}}$ or $k_{\mathrm{exp}}^{\mathrm{SSA}}$ in eqn (29) to results obtained directly from the pseudo-first order master equation by using eqn (11). We see that at the lowest pressure, both rate constants perfectly reproduce the master equation results. However, at 100 K and 10^7 Torr, $k_{\mathrm{exp}}^{\mathrm{f}}$ only matches well with the first-stage decay of the benchmark, during which RC does not accumulate significantly; $k_{\mathrm{exp}}^{\mathrm{f}}$ fails to reproduce the long-time behavior of the concentration – at long times the predictions from rate constants deviate dramatically from eqn (11). Results obtained using $k_{\mathrm{exp}}^{\mathrm{SSA}}$ do not reproduce well the first stage of the decay but are relatively closer to the benchmark in the whole considered time period. At high pressures (e.g., 10^7 Torr), the concentration of OH radical obtained from the master equation shows biexponential decay. This implies that the exponential decay constant for the title reaction is a good approximation only for low pressures or after an induction period.

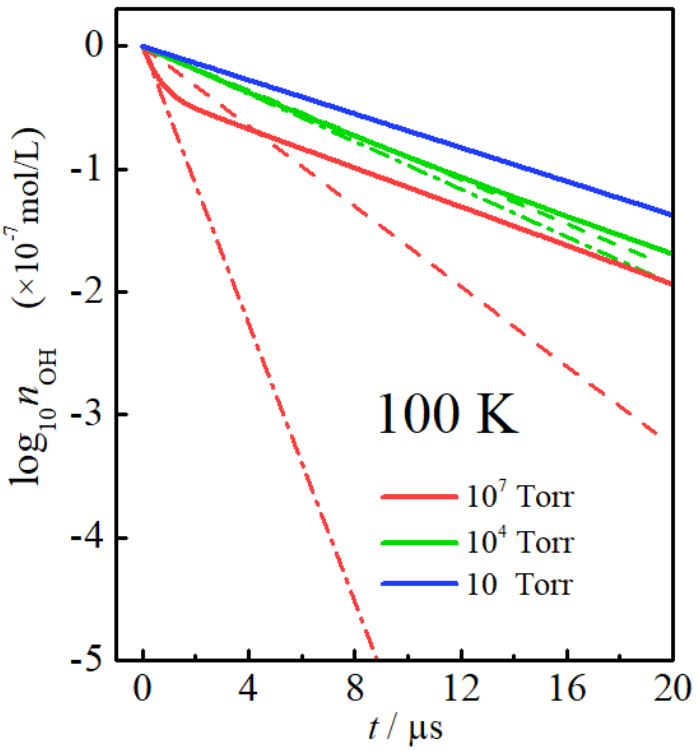

Figure 10. The concentration of OH as a function of time. The dashed lines are from $k_{\mathrm{exp}}^{\mathrm{SSA}}$, the dash-dot lines are from $k_{\mathrm{exp}}^{\mathrm{f}}$, and the solid lines are from time evolution of pseudo-first order master equation. The initial conditions are $n_{\mathrm{OH}}(t=0) = 10^{-7}$ mol/L, $n_{\mathrm{RC}}(t=0) = 0$, and $n_{\mathrm{HCHO}} \equiv 10^{-5}$ mol/L. Note that at 10 Torr, the dashed and dash–dot curves are hidden under the solid curve.

4.4.3 The ambiguous zone

The predictions of CSE theory depend on whether the reaction complex is viewed as merged

with the reactant. The threshold value for the merger is ambiguous. Thus for a given (T, p), some researchers may use the merged eqn (33), while others use the unmerged eqn (34) or (35) to calculate the experimentally observable rate constant. In the present work, we define the ambiguous zone for a given pressure to be temperatures in the range where P is between 0.2 and 0.6, that is, from $T_{\mathrm{m}}|_{P=0.2}$ to $T_{\mathrm{m}}|_{P=0.6}$. The ambiguous zones for p=10^{-2}, 10^{1}, 10^{4} and 10^{7} Torr are 200–300 K, 250–350 K, 300–450 K and 450–700 K, respectively. To examine the difference in rate constant predictions in the ambiguous zones, we list in Table 5 the ratios of experimentally observable rate constants estimated in the unmerged way to those calculated in the merged way. Results show that the choice of merger threshold barely affects the SSA rate constant but significantly affects the result if one estimates the experimentally observed rate constant by $k_{\mathrm{exp}}^{\mathrm{f}}$. Comparing (33) with (34) or (35), we see that the rate constant for the unmerged way contains an additional term involving RC and also the expression used for $k_{\mathrm{R}\to\mathrm{P}}$ is different, however, the difference between the merged and unmerged expressions for $k_{\mathrm{R}\to\mathrm{P}}$ (compare eqns (24) and (25)) is negligible in the ambiguous zone.

In the $k_{\mathrm{exp}}^{\mathrm{f}}$ expression, the RC term is the rate constant $k_{\mathrm{R}\to\mathrm{RC}}$, and in the $k_{\mathrm{exp}}^{\mathrm{SSA}}$ expression, it is $\frac{k_{\mathrm{R}\to\mathrm{RC}}k_{\mathrm{RC}\to\mathrm{P}}}{k_{\mathrm{RC}\to\mathrm{R}}+k_{\mathrm{RC}\to\mathrm{P}}}$; both of these are negligible for for $p \le 10^{4}$ Torr because $k_{\mathrm{R}\to\mathrm{RC}}$ is much less than $k_{\mathrm{R}\to\mathrm{P}}$. At a pressure of 10^{7} Torr, as can be seen in Figure 4, $k_{\mathrm{R}\to\mathrm{RC}}$ is much larger than $k_{\mathrm{R}\to\mathrm{P}}$ and the ratio $k_{\mathrm{exp}}^{\mathrm{f}}/k_{\mathrm{exp}}$ is significantly larger than 1. In the SSA, $k_{\mathrm{R}\to\mathrm{RC}}$ is multipled by $\frac{k_{\mathrm{RC}\to\mathrm{P}}}{k_{\mathrm{RC}\to\mathrm{R}}+k_{\mathrm{RC}\to\mathrm{P}}}$, and this makes the RC term negligible.

The SSA is robust in the ambiguous zone and avoids the sharp decay in $k_{\mathrm{exp}}^{\mathrm{f}}$ caused by the merger of R and RC (as the Figure S4 in the SI and Figure 3 of the ref. 25). We recommend using the SSA as the rate constant when comparing with experimental results for a bimolecular reaction proceeding to bimolecular products through a complex.

Table 5 Comparison of merged and unmerged calculations of rate constants[a]

	$k_{\mathrm{exp}}^{\mathrm{SSA}}/k_{\mathrm{exp}}$				$k_{\mathrm{exp}}^{\mathrm{f}}/k_{\mathrm{exp}}$			
T(K)/p(Torr)	10^{-2}	10^{1}	10^{4}	10^{7}	10^{-2}	10^{1}	10^{4}	10^{7}
250	1.00				1.00			
300	1.00	1.00			1.00	1.00		
350		1.00	1.01			1.00	1.03	
400			1.00				1.02	
450			1.00				1.01	
500				1.15				7.54
600				1.09				5.75
700				1.06				4.25

[a] $k_{\mathrm{exp}}^{\mathrm{SSA}}$ is from eqn (35) with rate constants $k_{\mathrm{R}\to\mathrm{P}}$ from eqn (24); k_{exp} is from eqn (33) with $k_{\mathrm{R}\to\mathrm{P}}$ from eqn (25); $k_{\mathrm{exp}}^{\mathrm{f}}$ is from eqn (34) with rate constants $k_{\mathrm{R}\to\mathrm{P}}$ from eqn (24).

4.4.4 The limiting cases

In the study of the methanol reaction with OH[66], we evaluated the high-pressure and low-pressure limits by using the canonical unified statistical (CUS) theory[68]. The reaction under study here is similar to that reaction in that both reactions have the complication of a reaction complex before a hydrogen-atom-transfer transition state. The CUS method predicts the experimentally observed reaction rate constants, but was originally designed to represent the low-pressure limit, i.e., the rate constant for reactions that are uninterrupted by third-body collisions. The rate constants we present above cover all pressure zones. Here we consider the relationship of CUS theory to the SSA, which was originally designed for situations where the reaction complex is a stabilized intermediate.

In this article, we do not consider reactions where there is path from reactants to products that does not pass over the reaction complex well. Then, in the high-pressure limit, reactive fluxes are due to reaction of stabilized and thermalized reaction complexes, and in the low-pressure limit, they result from reaction complexes flowing directly from reactant to product. Therefore the rate constant $k_{\mathrm{R}\to\mathrm{RC}}$ tends to the flux coefficients $\hat{k}_{\mathrm{R}\to\mathrm{RC}}$ in the high-pressure limit and tends to 0 in the low-pressure limit; and the rate constant $k_{\mathrm{R}\to\mathrm{P}}$ tends to 0 in the high-pressure limits[25]. As we illustrated above, the merger temperature T_{m} increases with pressure, and the RC can always be viewed as merged with R in the low-pressure limit and as a separate intermediate in the high-pressure limit. Based on these considerations, we can write down the low-pressure limit for the experimentally observable rate constant from eqn (33) as

$$k_{\mathrm{exp}}(p\to 0) = k_{\mathrm{R}\to\mathrm{P}} \tag{36}$$

and we can write down the high-pressure limit from eqns (34) and (35) as

$$k^{\mathrm{f}}_{\mathrm{exp}}(p\to\infty) = \hat{k}_{\mathrm{R}\to\mathrm{RC}} \tag{37}$$

$$k^{\mathrm{SSA}}_{\mathrm{exp}}(p\to\infty) = \frac{\hat{k}_{\mathrm{R}\to\mathrm{RC}}\hat{k}_{\mathrm{RC}\to\mathrm{P}}}{\hat{k}_{\mathrm{RC}\to\mathrm{R}} + \hat{k}_{\mathrm{RC}\to\mathrm{P}}} \tag{38}$$

Next we compare results of eqns (36), (37) and (38) with limiting cases of CUS theory.

1) *The high-pressure limits.* We will use the CUS theory with the approximation that the RC well is very deep; this yields[66]

$$k^{\mathrm{CUS}}(T) \approx \left(\frac{1}{\hat{k}_{\mathrm{R}\to\mathrm{RC}}(T)} + \frac{1}{\hat{k}_{\mathrm{RC}\to\mathrm{P}}(T)K_{\mathrm{R}\to\mathrm{RC}}}\right)^{-1} \tag{39}$$

where $K_{\mathrm{R}\to\mathrm{RC}}$ is the equilibrium constant for R→RC (equals the partition function of RC over the partition function of R). By construction, one has

$$\hat{k}_{\mathrm{RC}\to\mathrm{R}}(T) = \hat{k}_{\mathrm{R}\to\mathrm{RC}}(T)/K_{\mathrm{R}\to\mathrm{RC}} \tag{40}$$

Substituting eqn (40) into eqn (39) yields eqn (38), which shows that the SSA and CUS are consistent when the central well is very deep.

However, when the zero-point level of RC is lower than the zero-point level of R, as it is in the present case, both eqn (39) and eqn (40) implicitly assume the high-pressure limit because the calculation of $\hat{k}_{\mathrm{RC}\to\mathrm{R}}$ and $\hat{k}_{\mathrm{RC}\to\mathrm{P}}$ assumes that RC is equilibrated. In contrast, in the low-pressure limit, the appropriate ensemble for RC is a truncated canonical ensemble in which all energies below the zero-point level of R are removed from the RC ensemble because those energies of RC are inaccessible in the absence of stabilizing collisions. These missing energies are negative energies because in this whole article we place the zero of energy at the ground state of the reactant.

The above discussion shows that CUS theory with the assumption of a very deep well is equivalent to the SSA in the high-pressure limit (HPL).

2) *The low-pressure limits*. In low-pressure limit, we have[25]

$$k_{\mathrm{exp}}(p\to 0) = k_{\mathrm{R}\to\mathrm{P}}$$

$$= \frac{1}{h\Phi_{\mathrm{R}}^{\mathrm{rel}}}\int_0^{+\infty}\left(\frac{1}{\hat{k}_{\mathrm{R}\to\mathrm{RC}}(E)} + \frac{1}{\frac{\rho_{\mathrm{RC}}(E)}{\rho_{\mathrm{R}}(E)}\hat{k}_{\mathrm{RC}\to\mathrm{P}}(E)}\right)^{-1}\rho_{\mathrm{RC}}(E)e^{-\beta E}\mathrm{d}E \tag{41}$$

which is analogous to eqn (10b) of ref. 22. Here, the lower limit of integration is set at the zero-point level of the bimolecular reactant. Thus, as we have pointed out previously,[66,69] we do not include RC→P tunneling in the low-pressure limit for energies lower than the ground state of R.

Similarly, when we ignore the tunneling contribution in the low-pressure limit of CUS theory[66], we obtain

$$k^{\mathrm{CUS}}(T) \approx \left(\frac{1}{\hat{k}_{\mathrm{R}\to\mathrm{RC}}(T)} + \frac{1}{\hat{k}^{\mathrm{QC}}_{\mathrm{RC}\to\mathrm{P}}(T)K_{\mathrm{R}\to\mathrm{RC}}}\right)^{-1} \tag{42}$$

where the superscript 'QC' denotes "quasiclassical" which means tunneling is excluded in this flux coefficient (whereas when we do not mark a flux coefficient with superscript QC, it does include tunneling). As in previous articles[38,70,71,72,73,74] we label the result without tunneling as quasiclassical rather than classical because we still include quantum effects in the partition functions. Equation (41) and (42) are consistent except that the former is derived from microcanonical ensemble, and the latter is from the canonical ensemble.

We plotted results for the limiting cases, eqns (36), (37), (38), (39) and (42), in Figure 11. We observe that the low-pressure limit for CUS theory is slightly larger than high-pressure limits at high temperatures, which is due to the $\hat{k}^{\mathrm{QC}}_{\mathrm{RC}\to\mathrm{P}}(T)$ being slightly larger than $\hat{k}_{\mathrm{RC}\to\mathrm{P}}(T)$. (The former is calculated by CVT theory while the latter by CVT/SCT theory. The tunneling transmission coefficient [which accounts for both nonclassical transmission (i.e., tunneling) and nonclassical reflection (a diffraction effect)] is less than 1 in the CVT/SCT calculation because the effect of nonclassical reflection exceeds the effect of quantum mechanical tunneling, an effect that is sometimes observed for low-barrier or negative-barrier reactions.[75]

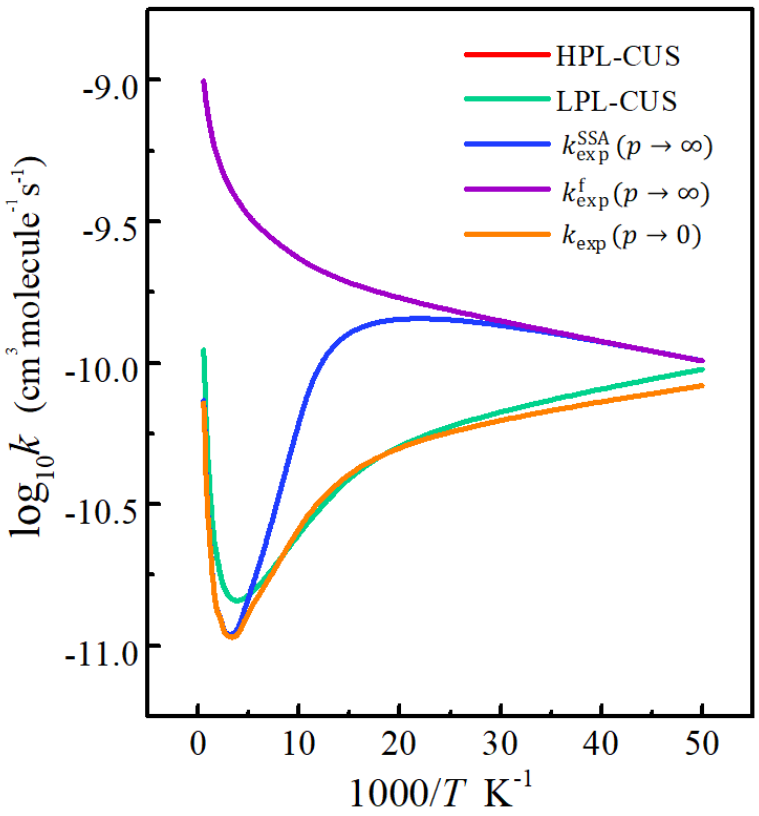

Figure 12. The limiting cases. HPL-CUS is calculated by eqn (39) and LPL-CUS is calculated by eqn (42).The curves for HPL-CUS and for $k_{\mathrm{exp}}^{\mathrm{SSA}}(p \to \infty)$ are overlapped.

5. Concluding remarks

The hydrogen abstraction reaction of HCHO by OH radical is a bimolecular reaction with a reverse reaction from a reaction complex. Pressure effects are often neglected in this kind of reaction. However, we find that the reaction complex RC formed by hydrogen-bonding interaction introduces a pressure effect on this reaction at low temperatures. Our study used a new version of our recently developed master equation program, *TUMME*, to solve the energy-resolved master equation. Phenomenological rate constants are extracted based on CSE theory. We use a pseudo-first order master equation in order to calculate the time evolutions of the concentrations. Both pressure activation and tunneling from the reaction complex to product can decrease the fraction of OH radical converted to the stabilized RC. Tunneling from the complex to the products affects the phenomenological reaction rate constants differently at high and low pressures and leads to a significant pressure effect.

To directly compare results with experiments, we defined two kinds of exponential decay constants: one neglects the reverse reactions, and the other one uses the steady-state approximation. Comparison of the decay curves of n_{OH} estimated using the two exponential decay constants with those from the direct master equation calculations show that exponential decay constant can reproduce the time-evolution of n_{OH} at low pressures but not at high pressures because n_{OH} decays in a biexponential way at high pressures.

ACKNOWLEDGMENTS

This work was supported in part by the National Natural Science Foundation of China (awards 21973053 and 91841301) and by the U.S. Department of Energy, Office of Science, Office of Basic Energy Sciences under Award DE-SC0015997.

References

1 S. Wang, D. F. Davidson and R. K. Hanson, High Temperature Measurements for the Rate Constants of C_1–C_4 Aldehydes with OH in a Shock Tube, *Proc. Combust. Inst.*, 2015, **35**, 473–480.

2 M. R. B. Abas and S. Mohamad, *Encyclopedia of Environmental Health* (Second Edition), edited by J. Nriagu, Elsevier, Oxford, 2011, pp. 405–416.

3 W. S. Snyder, M. R. Ford, G. G. Warner and H. L. Fisher Jr, *Estimates of Absorbed Fractions for Monoenergetic Photon Sources Uniformly Distributed in Various Organs of a Heterogeneous Phantom*, Oak Ridge National Lab., Oak Ridge, TN, 1969.

4 A. J. Ocaña, E. Jiménez, B. Ballesteros, A. Canosa, M. Antiñolo, J. Albaladejo, M. Agúndez, J. Cernicharo, A. Zanchet, P. del Mazo, O. Roncero and A. Aguado, Is the Gas-Phase OH + H_2CO Reaction a Source of Hco in Interstellar Cold Dark Clouds? *Astrophys. J.*, 2017, **850**, 28-40.

5 S. Xu, R. S. Zhu and M. C. Lin, Ab Initio Study of the OH + CH_2O Reaction: The Effect of the Oh·· Och2 Complex on the H-Abstraction Kinetics, *Int. J. Chem. Kinet.*, 2006, **38**, 322–326.

6 Y. Zhao, B. Wang, H. Li and L. Wang, Theoretical Studies on the Reactions of Formaldehyde with Oh and Oh, *J. Mol. Struct. Theochem*, 2007, **818**, 155–161.

7 P. d. Mazo-Sevillano, A. Aguado and O. Roncero, Neural Network Potential Energy Surface for the Low Temperature Ring Polymer Molecular Dynamics of the H_2CO + OH Reaction, *J. Chem. Phys.,* 2021, **154**, 094305-094319.

8 S. Zabarnick, J. W. Fleming and M. C. Lin, Kinetics of Hydroxyl Radical Reactions with Formaldehyde and 1, 3, 5-Trioxane between 290 and 600 K, *Int. J. Chem. Kinet.,* 1988, **20**, 117–129.

9 V. Sivakumaran, D. Hölscher and T. J. Dillon, Reaction between OH and HCHO: Temperature Dependent Rate Coefficients (202–399 K) and Product Pathways (298 K), *Phys. Chem. Chem. Phys.*, 2003, 5, 4821-4827.

10 V. Vasudevan, D. F. Davidson and R. K. Hanson, Direct Measurements of the Reaction OH +

$CH_2O \rightarrow HCO + H_2O$ at High Temperatures, *Int. J. Chem. Kinet.*, 2005, 37, 98–109.

11 B. D'Anna, V. Bakken, J. A. Beukes, C. J. Nielsen, K. Brudnik and J. T. Jodkowski, Experimental and Theoretical Studies of Gas Phase NO_3 and OH Radical Reactions with Formaldehyde, Acetaldehyde and Their Isotopomers, *Phys. Chem. Chem. Phys.*, 2003, **5**, 1790–1805.

12 M. A. Ali and J. R. Barker, Comparison of Three Isoelectronic Multiple-Well Reaction Systems: OH + CH_2O, OH + CH_2CH_2, and OH + CH_2NH, *J. Phys. Chem. A*, 2015, **119**, 7578–7592.

13 E. E. Wait, A. E. Masunov and S. S. Vasu, Quantum Chemical and Master Equation Study of OH + $CH_2O \rightarrow H_2O$+ CHO Reaction Rates in Supercritical CO_2 Environment, *Int. J. Chem. Kinet.*, 2019, **51**, 42-48.

14 G. d. S. Machado, E. M. Martins, L. Baptista and G. F. Bauerfeldt, Prediction of Rate Coefficients for the H_2CO + OH$\rightarrow$ HCO + H_2O Reaction at Combustion, Atmospheric and Interstellar Medium Conditions, *J. Phys. Chem. A*, 2020, **124**, 2309–2317.

15 R. M. Zhang, X. Xu and D. G. Truhlar, TUMME: Tsinghua University Minnesota Master Equation Program, *Computer Phys. Commun.,* 2021, **270**, 108140.

16 R. M. Zhang, X. Xu and D. G. Truhlar, *TUMME* computer program, version 3.0, https://comp.chem.umn.edu/tumme

17 B. J. Zwolinski and H. Eyring, The Non-Equilibrium Theory of Absolute Rates of Reaction, *J. Am. Chem. Soc.*, 1947, **69**, 2702-2707.

18 S. C. Smith, M. J. McEwan and R. G. Gilbert, The Relationship Between Recombination, Chemical Activation and Unimolecular Dissociation Rate Coefficients, *J. Phys. Chem.*, 1989, **90**, 4265-4273.

19 R. G. Gilbert and S. C. Smith, *Theory of Unimolecular and Recombination Reactions*, Blackwell Scientific Publishers, Oxford, 1990, pp. 268.

20 T. J. Frankcombe, S. C. Smith, K. E. Gates and S. H. Robertson, A Master Equation Model for Bimolecular Reaction Via Multi-Well Isomerizing Intermediates. *Physical Chemistry Chemical Phys., 2000, 2*, 793-803.

21 J. R. Barker, Multiple-Well, Multiple-Path Unimolecular Reaction Systems. I. MultiWell Computer Program Suite, *Int. J. Chem. Kinet*., 2001, **33**, 232-245.

22 J. A. Miller and S. J. Klippenstein, The Reaction between Ethyl and Molecular Oxygen II: Further Analysis, *Int. J. Chem. Kinet*., 2001, **33**, 654–668.

23 J. A. Miller and S. J. Klippenstein, From the Multiple-Well Master Equation to Phenomenological Rate Coefficients: Reactions on a C_3H_4 Potential Energy Surface, *J. Phys.*

Chem. A, 2003, **107**, 2680-2692.

24 A. Fernández-Ramos, J. A. Miller, S. J. Klippenstein and D. G. Truhlar, Modeling the Kinetics of Bimolecular Reactions, *Chem. Rev.*, 2006, **106**, 4518-4584.

25 J. A. Miller and S. J. Klippenstein, Master Equation Methods in Gas Phase Chemical Kinetics, *J. Phys. Chem. A*, 2006, **110**, 10528-10544.

26 Y. Georgievskii, J. A. Miller, M. P. Burke and S. J. Klippenstein, Reformulation and Solution of the Master Equation for Multiple-Well Chemical Reactions, *J. Phys. Chem. A*, 2013, **117**, 12146−12154.

27 S. J. Klippenstein, V. S. Pande and D. G. Truhlar, Chemical Kinetics and Mechanisms of Complex Systems: A Perspective on Recent Theoretical Advances, *J. Am. Chem. Soc.,* 2013, **136**, 528-546.

28 S. J. Klippenstein, J. A. Miller and A. W. Jasper, Kinetics of propargyl radical dissociation. *J. Phys. Chem. A,* 2015*,* **119**, 7780-7791.

29 B. Widom, Transitions and Chemical Reaction Rates, *Science,* 1965, **148**, 1555-1560.

30 B. C. Garrett and D. G. Truhlar, Criterion of Minimum State Density in the Transition State Theory of Bimolecular Reactions, *J. Chem. Phys.*, 1979, **70**, 1593-1598.

31 Y.-P. Liu, G. C. Lynch, T. N. Truong, D.-h. Lu, D. G. Truhlar and B. C. Garrett, Molecular Modeling of the Kinetic Isotope Effect for the [1, 5]-Sigmatropic Rearrangement of *cis*-1, 3-Pentadiene, *J. Am. Chem. Soc.*, 1993, **115**, 2408-2415.

32 D. G. Truhlar and B. C. Garrett, Variational Transition-State Theory, *Acc. Chem. Res.*, 1989, **13**, 440-448.

33 D. G. Truhlar, Tunneling in Enzymatic and Nonenzymatic Hydrogen Transfer Reactions, *J. Phys. Org. Chem.,* 2010, **23**, 660-676.

34 J. Zheng, T. Yu, E. Papajak, I, M. Alecu, S. L. Mielke and D. G. Truhlar, Practical Methods for Including Torsional Anharmonicity in Thermochemical Calculations on Complex Molecules: The Internal-Coordinate Multi-Structural Approximation, *Phys. Chem. Chem. Phys.,*2011, **13**, 10885–10907.

35 D. Osborn, Reaction Mechanisms on Multiwell Potential Energy Surfaces in Combustion (and Atmospheric) Chemistry, *Annu. Rev. Phys. Chem.*, 2017, **68**, 233-260.

36 A. P. Penner and W. Forst, Analytic Solution of Relaxation in a System with Exponential Transition Probabilities, *J. Chem. Phys.*, 1977, **67**, 5296-5307.

37 T. Yu, J. Zheng and D. G. Truhlar, Multi-Structural Variational Transition State Theory. Kinetics of the 1, 4-Hydrogen Shift Isomerization of the Pentyl Radical with Torsional Anharmonicity, *Chem. Sci*., 2011, **2**, 2199-2213.

38 J. L. Bao and D. G. Truhlar, Variational Transition State Theory: Theoretical Framework and Recent Developments, *Chem. Soc. Rev.,* 2017, **46**, 7548-7596.

39 S. Glasstone, K. J. Laidler and H. Eyring, *The Theory of Rate Processes*, McGraw-Hill, New York, 1941.

40 J. Zheng, S. L. Mielke, J. L. Bao, R. Meana-Pañeda, K. L. Clarkson and D. G. Truhlar, *MSTor* computer program, version 2017, University of Minnesota, Minneapolis, MN, 2017.

41 S. H. Lin and H. Eyring, Improved Calculation of Quasiequilibrium Reaction Rate Constants, *J. Chem. Phys.*, 1963, **39**, 1577-1579.

42 S. H. Lin and H. Eyring, Calculation of Statistical Complexions of Harmonic Oscillations, *J. Chem. Phys.*, 1965, **43**, 2153.

43 M. R. Hoare,. W. Ruijgrok, Inversion of the Partition Function: The First-Order Steepest-Descent Method, *J. Chem. Phys.* 1970, **52**, 113-120.

44 W. Forst, *Unimolecular Reactions: A Concise Introduction,* Cambridge University Press, Cambridge, 2003, pp. 82.

45 W. Forst, *Theory of Unimolecular Reactions*, Academic Press, New York, 1973, pp.109.

46 J. A. Miller and S. J. Klippenstein, Determining Phenomenological Rate Coefficients from a Time-Dependent, Multiple-Well Master Equation: "Species Reduction" at High Temperatures，*Phys. Chem. Chem. Phys.,* 2013, **15**, 4744-4753.

47 R. M. Zhang, X. Xu and D. G Truhlar, Low-Pressure Limit of Competitive Unimolecular Reactions, *J. Am. Chem. Soc.* 2020**, 142**, 16064-16071.

48 T. J. Lee and P. R. Taylor, A Diagnostic for Determining the Quality of Single-Reference Electron Correlation Methods, *Int. J. Quantum Chem.* 1989, **23**, 199- 207.

49 T. J. Lee, J. E. Rice, G. E. Scuseria and H. F. Schaefer, Theoretical Investigations of Molecules Composed Only of Fluorine, Oxygen and Nitrogen: Determination of the Equilibrium Structures of FOOF, $(NO)_2$ and FNNF and the Transition State Structure for FNNF *cis–trans* Isomerization, *Theor. Chim. Acta*, 1989, **75**, 81-98.

50 P. J. Knowles, C. Hampel, and H. J. Werner, Coupled cluster theory for high spin, open shell reference wave functions, *J. Chem. Phys.*, 1993, **99**, 5219–5227; Erratum: *J. Chem. Phys.*, 2000, **112**, 3106-3107.

51 E. Papajak and D. G. Truhlar, Convergent Partially Augmented Basis Sets for Post-Hartree−Fock Calculations of Molecular Properties and Reaction Barrier Heights, *J. Chem. Theory Comput.*, 2011, **7**, 10–18.

52 E. Papajak, J. Zheng, X. Xu, H. R. Leverentz and D. G. Truhlar, Perspectives on Basis Sets Beautiful: Seasonal Plantings of Diffuse Basis Functions, *J. Chem. Theory Comput.*, 2011, **7**, 3027–3034.

53 Y. Zhao and D. G. Truhlar, Exploring the Limit of Accuracy of the Global Hybrid Meta Density Functional for Main-Group Thermochemistry, Kinetics, and Noncovalent Interactions, *J. Chem. Theory Comput.* 2008, ***4***, 1849-1868.

54 X. Xu, I. M. Alecu and D. G. Truhlar, How Well Can Modern Density Functionals Predict Internuclear Distances at Transition States? *J. Chem. Theory Comput.* 2011, **7**, 1667−1676.

55 X. Li, X. Xu, X. You and D. G. Truhlar, Benchmark Calculations for Bond Dissociation Enthalpies of Unsaturated Methyl Esters and the Bond Dissociation Enthalpies of Methyl Linolenate, *J. Phys. Chem. A*, 2016, **120**, 4025−4036.

56 R. Meana-Pañeda, X. Xu, H. Ma and D. G. Truhlar, Computational Kinetics by Variational Transition-State Theory with Semiclassical Multidimensional Tunneling: Direct Dynamics Rate Constants for the Abstraction of H from CH_3OH by Triplet Oxygen Atoms, *J. Phys. Chem. A*, 2017, **121**, 1693−1707.

57 R. A. Kendall, T. H. Dunning Jr. and R. J. Harrison, Electron Affinities of the First-Row Atoms Revisited. Systematic Basis Sets and Wave Functions, *J. Chem. Phys.* 1992**, *96***, 6796-6806.

58 I. M. Alecu, J. Zheng, Y. Zhao and D. G. Truhlar, Computational Thermochemistry: Scale Factor Databases and Scale Factors for Vibrational Frequencies Obtained from Electronic Model Chemistries, *J. Chem. Theory Comput.* 2010, **6**, 2872−2887.

59 G. Knizia,T. B. Adler and H.-J. Werner, Simplified CCSD (T)-F12 Methods: Theory and Benchmarks, *J. Chem. Phys.*, 2009, **130**, 054104-054124.

60 K. Raghavachari, G. W.Trucks, J. A. Pople and M. A. Head-Gordon. A Fifth-Order Perturbation Comparison of Electron Correlation Theories, *Chem. Phys. Lett.*, 1989, **157**, 479−483.

61 M. J. Frisch, G. W. Trucks, H. B. Schlegel, G. E. Scuseria, M. A. Robb, J. R. Cheeseman, G. Scalmani, V. Barone, G. A. Petersson, H. Nakatsuji, X. Li, M. Caricato, A. V. Marenich, J. Bloino, B. G. Janesko, R. Gomperts, B. Mennucci, H. P. Hratchian, J. V. Ortiz, A. F. Izmaylov, J. L. Sonnenberg, D. Williams-Young, F. Ding, F. Lipparini, F. Egidi, J. Goings, B. Peng, A. Petrone, T. Henderson, D. Ranasinghe, V. G. Zakrzewski, J. Gao, N. Rega, G. Zheng, W. Liang, M. Hada, M. Ehara, K. Toyota, R. Fukuda, J. Hasegawa, M. Ishida, T. Nakajima, Y. Honda, O. Kitao, H. Nakai, T. Vreven, K. Throssell, J. A. Montgomery, Jr., J. E. Peralta, F. Ogliaro, M. J. Bearpark, J. J. Heyd, E. N. Brothers, K. N. Kudin, V. N. Staroverov, T. A. Keith, R. Kobayashi, J. Normand, K. Raghavachari, A. P. Rendell, J. C. Burant, S. S. Iyengar, J. Tomasi, M. Cossi, J. M. Millam, M. Klene, C. Adamo, R. Cammi, J. W. Ochterski, R. L. Martin, K. Morokuma, O. Farkas, J. B. Foresman and D. J. Fox, *Gaussian 16* computer program, revision b01, Gaussian, Inc., Wallingford CT, 2016.

62 H.-J. Werner, P. J. Knowles, G. Knizia, F. R. Manby, M. Schütz, P. Celani, T. Korona, R. Lindh, A. Mitrushenkov, G. Rauhut, K. R. Shamasundar, T. B. Adler, R. D. Amos, A. Bernhardsson, A. Berning, D. L. Cooper, M. J. O. Deegan, A. J. Dobbyn, F. Eckert, E. Goll,

C. Hampel, A. Hesselmann, G. Hetzer,, T. Hrenar G. Jansen C. , Köppl, Y. Liu, A. W. Lloyd, R. A. Mata, A. J. May, S. J. McNicholas, W. Meyer, M. E. Mura, A. Nicklass, D. P. O'Neill,)P. Palmieri, D. Peng, K. Pflüger, R. Pitzer, M. Reiher, T. Shiozaki, H. Stoll, A. J. Stone, R. Tarroni, T. Thorsteinsson and M. Wang, *Molpro* computer program, version 2015.1, University of Birmingham, Birmingham, 2015.

63 J. Zheng, J. L. Bao, S. Zhang, J. C. Corchado, R. Meana-Pañeda, Y.-Y. Chuang, E. L. Coitiño, B. A. Ellingson and D. G. Truhlar, *Gaussrate 17* computer program, University of Minnesota, Minneapolis, MN, 2017.

64 J. Zheng, J. L. Bao, R. Meana-Pañeda, S. Zhang, B. J. Lynch, J. C. Corchado, Y.-Y. Chuang, P. L. Fast, W.-P. Hu, Y.-P. Liu, G. C. Lynch, K. A. Nguyen, C. F. Jackels, A. Fernandez Ramos, B. A. Ellingson, V. S. Melissas, J. Villà, I. Rossi, E. L. Coitiño, J. Pu, T. V. Albu, A. Ratkiewicz, R. Steckler, B. C. Garrett, A. D. Isaacson and D. G. Truhlar, *Polyrate* computer program, version 2017-C, University of Minnesota, Minneapolis, MN, 2017.

65 R. Cambi, D. Cappelletti, G. Liuti and F. Pirani, Generalized Correlations in Terms of Polarizability for Van Der Waals Interaction Potential Parameter Calculations, *J. Chem. Phys.*, 1991, **95**, 1852-1862

66 L. G. Gao, J. Zheng, A. Fernández-Ramos, D. G. Truhlar and X. Xu, Kinetics of the Methanol Reaction with Oh at Interstellar, Atmospheric, and Combustion Temperatures, *J. Am. Chem. Soc.,* 2018, **140**, 2906-2918.

67 H. G. Hammes, *Principles of Chemical Kinetics*, Academic Press, New York, 1978, pp. 11.

68 B. C. Garrett and D. G. Truhlar, Canonical Unified Statistical Model. Classical Mechanical Theory and Applications to Collinear Reactions, *J. Chem. Phys.*, 1982, **76**, 1853-1858.

69 J. Zheng and D. G. Truhlar, Multi-path variational transition state theory for chemical reaction rates of complex polyatomic species: ethanol+ OH reactions., *Faraday Discuss.*, 2012, **157**, 59-88.

70 D. G. Truhlar and J. R. Pliego Jr., in *Continuum Solvation Models in Chemical Physics: From Theory to Applications,* edited by B. Mennucci and R. Cammi (Wiley, Chichester, 2008), pp. 338-365.

71 L. Masgrau and D. G. Truhlar, The importance of ensemble averaging in enzyme kinetics, *Acc. Chem. Res.,* 2015, **48**, 431-438.

72 J. Zheng, G. Odeyepo and D. G. Truhlar, Kinetics of the hydrogen abstraction reaction from 2-butanol by OH radical., *J. Phys. Chem. A*, 2015, **117**, 12182-12192.

73 L. Xing, J. L. Bao, Z. Wang, X. Wang and D. G. Truhlar, Relative rates of hydrogen shift isomerizations depend strongly on multiple-structure anharmonicity, *J. Am. Chem. Soc.*, 2018, **140**, 17556-17570.

74 D. G. Truhlar, in *Tunnelling in Molecules: Nuclear Quantum Effects from Bio to Physical Chemistry*, edited by J. Kaestner and S. Kozuch, RSC Publishing, Cambridge, 2021, pp. 261-

282.

75 W.-P. Hu, I. Rossi, J. C. Corchado, and D. G. Truhlar, Molecular modeling of combustion kinetics. The abstraction of primary and secondary hydrogens by hydroxyl radical, *J. Phys. Chem. A*, 1997, **101**, 6911-6921.